Land use and anthropogenic heat modulate ozone by meteorology: A perspective from the Yangtze River Delta region

Chenchao Zhan [a], Min Xie [a,*]

[a] School of Atmospheric Sciences, CMA-NJU Joint Laboratory for Climate Prediction Studies, Jiangsu Collaborative Innovation Center for Climate Change, Joint Center for Atmospheric Radar Research of CMA/NJU, Nanjing University, Nanjing 210023, China

---

[*] Corresponding author. minxie@nju.edu.cn (M. Xie)

Abstract: With the rapid advance in urbanization, land use and anthropogenic heat (AH) dictated by human activities significantly modify the urban climate and in turn the air quality. Focusing on the Yangtze River Delta (YRD) region, a highly urbanized coastal area with severe ozone (O_3) pollution, we estimate the impacts of land use and AH on meteorology and O_3 using the WRF-Chem model. These results enhance our understanding of the formation of O_3 pollution in rapidly developing city clusters with place-specific topography, as most of our results can be supported by previous studies conducted in other regions around the world. Regional O_3 pollution episodes occur frequently (~26 times per year) in the YRD from 2015 to 2019. These O_3 pollution episodes are usually in calm conditions characterized by high temperature (over 20 ℃), low relative humidity (less than 80%), light wind (less than 3 m s^{-1}) and shallow cloud cover (less than 5 okta). In this case, O_3 pollution belts tend to appear in the converging airflows associated with the sea and the lake breezes. On the other hand, rapid urbanization has significantly changed land use and AH in this region, which subsequently affects the meteorology and O_3 concentration. The largest change in land use comes from urban expansion, which causes an increase in 2-m temperature (T_2) by a maximum of 3 ℃, an increase in planetary boundary layer height (PBLH) by a maximum of 500 m, a decrease in 10-m wind speed (WS_{10}) by a maximum of 1.5 m s^{-1} and an increase in surface O_3 by a maximum of 20 μg m^{-3}. With regard to the sea and lake breezes, the expansion of coastal cities, like Shanghai, can enhance the sea breeze circulation by ~1 m s^{-1}. During the advance of the sea breeze front inland, the updraft induced by the front makes well vertical mixing of O_3. However, once the sea breeze is fully-developed in the afternoon (~17:00

LT), further progression inland will ~~be~~ stall~~ed~~. Then ~~the~~ O_3 removal by the low sea breeze will be weakened, and surface O_3 can be 10 μg m^{-3} higher in the case with cities than no-cities. The expansion of lakeside cities, ~~like~~ such as Wuxi and Suzhou, can extend the lifetime of ~~the~~ lake breezes from noon to afternoon. Since the offshore flow of the lake breeze transports high O_3 from the land to the lake, the onshore flow brings ~~the~~ high O_3 back to the land. Surface O_3 in lakeside cities can increase as much as 30 μg m^{-3}. Compared to land use, the effects of AH are relatively small. ~~And t~~The changes mainly appear in and around cities where AH fluxes are large. There are increases in T_2, PBLH, WS_{10} and surface O_3 when AH fluxes are taken into account, with ~~the~~increments of approximately ~~increment of about~~ 0.2 °C, 75 m, 0.3 m s^{-1} and 4 μg m^{-3}, respectively. AH contributes largely to the urban environment, altering meteorological factors, O_3 concentration and urban breeze circulation, but its effect on the sea and the lake breezes seems to be limited.

Key Words: ozone; local circulations; land use; anthropogenic heat; the Yangtze River Delta;

1 Introduction

~~Ozone (O_3) is a key constituent in the atmosphere, but acts quite differently in different parts of the atmosphere, often described as being "good up high and bad nearby". O_3 in the stratosphere helps protect life on earth from strong ultraviolet radiation. However, high O_3 in the troposphere is harmful to human respiratory system (Jerrett et al., 2009), the growth of vegetation (Mills et al., 2011) and climate (Worden et al., 2008). Therefore, tropospheric O_3 has long been regarded as an important air pollutant and has received continuous attention within the last few decades.~~

~~Tropospheric~~ Tropospheric O_3 is a secondary pollutant ~~mainly~~ formed by a series of complex chemical reactions (Chameides and Walker, 1973; Xie et al., 2014) of precursor gases such as nitrogen oxides (NO_x=NO+NO_2) and volatile organic compounds (VOCs) in combination with sunlight. It has received continuous attention within the last few decades due to its negative effects on human respiratory system (Jerrett et al., 2009) and the growth of vegetation (Mills et al., 2011). The global average lifetime of tropospheric ~~tropospheric~~ O_3 is 20 to 25 days, and it will decrease~~reduce~~ to 5 days in the boundary layer (Young et al., 2013). The relatively long lifetime of ~~tropospheric~~ O_3 favors regional/long-range transport~~,~~ and brings huge challenges to its control (Bergin et al., 2005). O_3 concentrations~~levels~~ considerably depend on ~~the~~ weather conditions because they play an important role in determining the chemistry, dispersion and removal of O_3

(Jacob and Winner, 2009). ~~In general, e~~Elevated O_3 usually occurs under warm dry weather with strong sunlight, high temperature, low relative humidity and light wind speed (Zhang et al., 2015). Furthermore, weather conditions have many similarities in certain weather pattern (Buchholz et al., 2010; Zhan et al., 2019), and the main weather patterns associated with O_3 pollution episodes in China are tropical cyclones and continental anticyclones (Wang et al., 2017).

O_3 concentration~~s as well as~~and meteorology in urban areas are of great concern ~~simply~~ because urban areas have huge populations~~because urban areas have huge populations~~. A report from the United Nations pointed out that 69.6% of the world's population will live in cities by 2050. ~~The urbanization process has also increased urban environmental hazards (Zhang et al., 2011), particularly in the most rapidly developing countries like China (Liu and Tian, 2010).~~ Because of historical and cultural factors, many cities have similar topography, usually along the coasts, close to mountains or in basins. For these cities, the local circulations induced by thermal contrast of the topography, such as sea-land breezes, mountain-valley breezes and lake-land breezes, have an important impact on urban air quality~~, especially~~ under calm conditions~~weak synoptic forcing~~ (Crosman and Horel, 2010). Examples can be found around the world. Ding et al. (2004) simulated the main features of sea-land breezes during a multiday episode in the Pearl River Delta (PRD) region, and found that the sea-land breezes can transport air pollutants between inland and coastal cities. Miao et al. (2015) studied the effects of mountain-valley breezes on the boundary layer structure in the Beijing-Tianjin-Hebei (BTH) region, suggesting that ~~the~~ mountain-valley breezes are vital to the vertical transport and distribution of air pollutants in Beijing. Wentworth et al. (2015) identified a causal link between lake breezes and O_3 in the Greater Toronto Area that the daytime O_3 maxima were~~as~~ 13.6-14.8 ppb higher on lake breeze days than on no-lake breeze days.

Ongoing urbanization~~Human activities~~, ~~such as~~ including changes in land use and anthropogenic heat (AH), ~~contribute to changes of~~can affect meteorology and atmospheric compositions at local, regional and even global scales (Fu and Liao, 2014; Park et al., 2014; Oke et al., 2017). Land use changes via urban expansion (typically from vegetation to impervious surface) directly alter~~s~~ the surface physical properties (e.g., albedo, surface moisture and roughness), subsequently affecting the exchange of energy, moisture and momentum, and hence impacting the urban climate and air quality (Jiang et al., 2008; Wang et al., 2009). Li et al. (2019) found that increases in thermal inertia, surface roughness and evapotranspiration due to urban expansion can

rise O_3 by 5.6 ppb in Southern California. AH is an important waste by-product of urban metabolism. Nearly all energy consumed by human activities will be dissipated as heat within Earth's land-atmosphere system (Flanner, 2009; Sailor, 2011), which ~~that~~ is then "injected" into the energy balance processes. Ryu et al. (2013~~a~~) reported that AH affects the characteristics/structures of the boundary layer and local circulations, resulting in an increase in~~of~~ O_3 by 3.8 ppb in the Seoul metropolitan area.

Previous studies usually investigated the impacts of topography, land use and AH on meteorology and air quality separately, and mainly focused~~sing~~ on a specific megacity. However, these factors can work together in near-calm conditions. Furthermore, complex interactions exist widely among ~~these~~ thermally ~~-~~driven circulations, and the effects can even spread from one city to nearby areas. For example, Zhu et al. (2015) demonstrated that the meteorological conditions and air quality over Kunshan are significantly affected by Shanghai urban land surface forcing (Kunshan is located downstream of Shanghai~~,~~ with a straight-line distance of approximately~~about~~ 50 km). Given the increasing prevalence of cities, cities gradually appear in the form of clusters. Therefore, assessing the effects of land use and AH (the ~~the~~ topography rarely changes.) in ~~the~~ city clusters is meaningful, which also helps understand the interactions between the urban environment and human activities.

The Yangtze River Delta (YRD) region, located on the western coast of the Pacific Ocean (Figure 1a), has undergone accelerated urbanization processes and rapid economic development over the past few decades. It is now one of the largest economic zones in the world. The YRD region consists of the southern part of Jiangsu Province, the northern part of Zhejiang Province and the eastern part of Anhui Province, including 26 mega/large cities such as Shanghai, Hangzhou and Nanjing (Figure 1b). With dense population and huge energy consumption, this area is now suffering from air quality deterioration (Xie et al., 2017; Zhan et al., 2020), especially the increasingly severe O_3 pollution in recent years (Li et al., 2020; Wang et al., 2020). Furthermore, cities with hot spots of O_3 are usually concentrated~~concentrate~~ in the central YRD region~~,~~ surrounding Tai Lake (Zhan et al., 2021). Numerous cities, unique topography and severe~~sever~~ O_3 pollution make the YRD an ideal study place.

In this study, the impacts of land use and AH on meteorology in the central YRD region, and how these effect~~impact~~s further modulate O_3 are investigated using the Weather Research and

Forecasting model coupled to Chemistry (WRF-Chem). These results fill the knowledge gap about the formation of O_3 pollution in this region and provide valuable insight for other rapidly developing regions with complex topography in the world. The remainder of this paper is organized as follows. Sect. 2 gives a detailed description ~~about~~ of the observation data, the model setup and the experimental design. The main results, including the characteristics of O_3 pollution episodes, the model evaluation and the changes in meteorology and O_3 caused by land use and AH, are presented in Sect. 3. Summary and conclusions are given in Sect. 4.

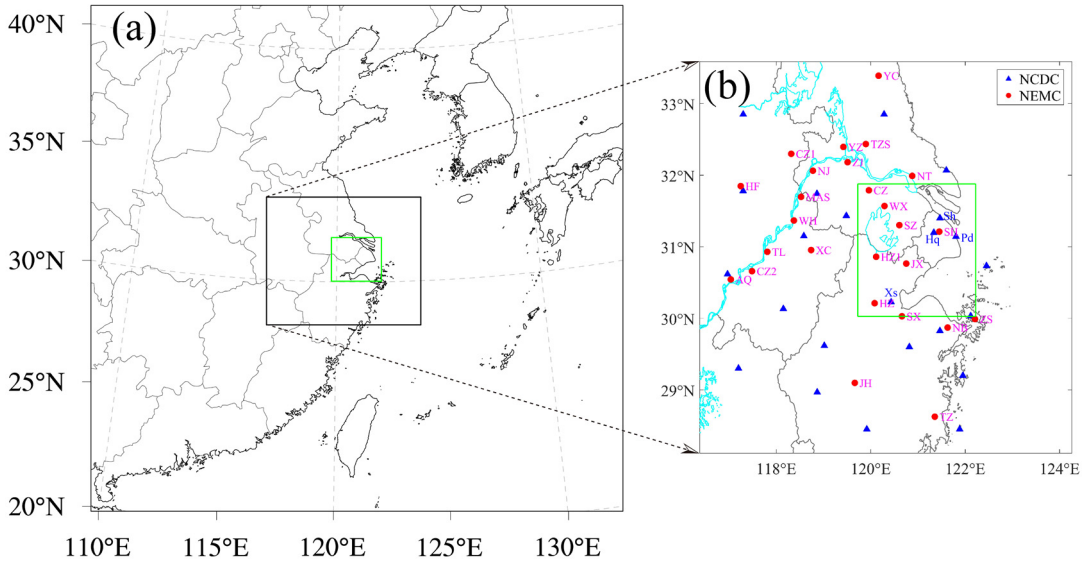

Figure 1. (a) Three nested WRF-Chem domains~~,~~. (b) ~~the~~ The locations of ~~26~~ cities (red dots) and weather stations (blue triangles) in the YRD. The green rectangular regions represent the innermost domain and also the central YRD region. The~~se~~ cities in (b) include: the megacity Shanghai (SH); Hangzhou (HZ), Ningbo (NB), Jiaxing (JX), Huzhou (HZ1), Shaoxing (SX), Jinhua (JH), Zhoushan (ZS) and Taizhou (TZ) located in Zhejiang Province; Nanjing (NJ), Wuxi (WX), Changzhou (CZ), Suzhou (SZ), Nantong (NT), Yancheng (YC), Yangzhou (YZ), Zhenjiang (ZJ) and Taizhoushi (TZS) located in Jiangsu Province; and Hefei (HF), Wuhu (WH), Maanshan (MAS), Tongling (TL), Anqing (AQ), Chuzhou (CZ1), Chizhou (CZ2) and Xuancheng (XC) located in Anhui Province.

2 Materials and methods

2.1 Surface observations

Hourly O_3 concentrations monitored by the National Environmental Monitoring Center (NEMC) of China are used in this study. These data strictly follow the national monitoring standards HJ 654-2013 and HJ 193-2013 (http://www.cnemc.cn/jcgf/dqhj/)~~,~~ and are~~can be~~ available at https://quotsoft.net/air/. The nationwide observation network initially operated in 74 major cities since 2013, and it has grown to more than 1,500 stations covering 454 cities by 2017 (Lu et al., 2018). The urban hourly O_3 concentrations are the average results of measurements at all monitoring sites in that~~for each~~ city. The ~~maximum~~ daily maximum 8-h~~ running~~ average (MDA8) O_3 concentrations are~~ then~~ calculated using~~based on~~ the hourly O_3 concentrations for days with more than 18-h measurements~~ in the day~~ (Liao et al., 2017).

Meteorological data are taken from~~provided by~~ the National Climatic Data Center (NCDC), including 2-m air temperature (T_2), relative humidity (RH), 10-m wind speed (WS_{10}) and direction (WD_{10}) and cloud cover (CC). These data as well as the technical documents recording the quality control, data collection and archive ~~can be~~are available at ftp://ftp.ncdc.noaa.gov/pub/data/noaa/isd-lite/. Locations of the ~~surface observation~~weather stations are shown in Figure 1b. Specifically, the ~~meteorological~~ weather stations in the innermost domain ~~include~~ are Pudong (Pd), Shanghai (Sh), Hongqiao (Hq) and Xiaoshan (Xs).

2.2 MODIS-based and USGS land use classifications

To explore the effects of land use~~ on meteorology and O_3 in the YRD~~, two land use categories defaulted in WRF are used to set up the first two scenario~~scenarios~~ simulations (Table 2). The MODIS-based land cover product was created from 500-m MODIS Terra and Aqua satellite imagery (Friedl et al., 2010)~~,~~ and replaced USGS as the default settings in WRF since version 3.8. The USGS data were primarily derived from the Advanced Very High Resolution Radiometer (AVHRR) from 1992 to 1993 at 1-km spatial resolution (Loveland et al., 2000), which reflects the distribution of cities in the late 1980s. Figure 2 presents the land cover maps in the innermost domain. The most obvious difference between MODIS and USGS is~~ comes from~~ the urban fraction, which is related to the urban expansion caused by rapid urbanization~~ in recent decades in the YRD~~. In addition, the Finer Resolution Observation and Monitoring-Global Land Cover in 2015 (GLC), ~~which is~~ one of the latest (2015) and finest (30-m) land cover datasets (Gong et al., 2019), is quite consistent with the performance of MODIS in this region. This confirms that the urban fraction in MODIS is close to~~ the~~ reality. Thus, the MODIS data can generally refer to today's distribution of cities.

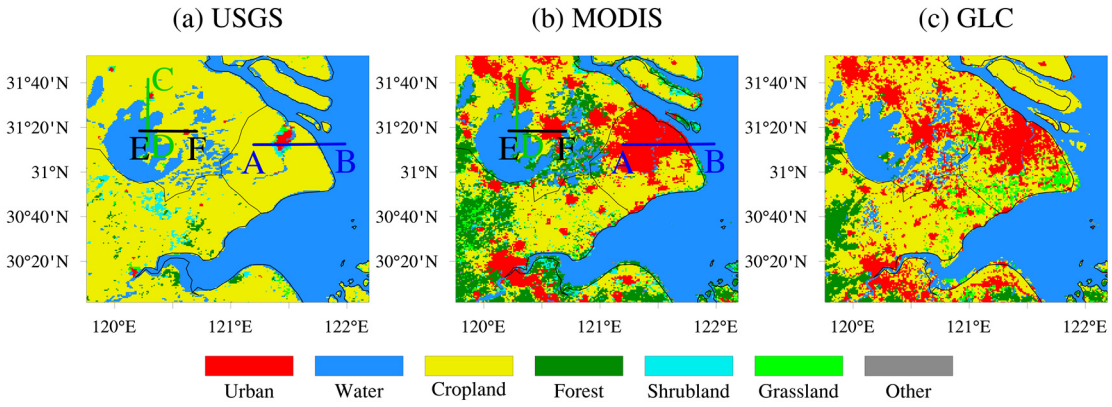

Figure 2. Land cover maps in the innermost domain, ~~including the result of~~with (a) USGS, (b) MODIS, and (c) GLC datasets.

2.3 Anthropogenic heat flux modeling

Another scenario simulation incorporates the urban canopy model with ~~the~~ gridded AH fluxes to diagnose the impact of AH. The AH fluxes were calculated based on the ~~statistics~~ statistical data of energy consumption of China in 2016, and then were grided as 144 rows and 144 columns with a resolution of~~at~~ 2.5° using population density downloaded from Columbia University's Socioeconomic Data and Applications Center. AH fluxes with their diurnal variations are considered by adding them to the sensible heat flux from the urban canopy layer within the Single Layer Urban Canopy Model (SLUCM). The AH fluxes for each grid are determined by the fixed AH value for the urban land use category, the urban fraction value on each grid and the fixed temporal diurnal pattern. Details on the calculation of AH fluxes, and how to add AH fluxes into the model can ~~refer to~~be found in Xie et al. (2016a, b). Figure 3 gives the spatial distribution of AH fluxes in the innermost domain. In ~~the~~ urban ~~–~~areas, the AH fluxes usually exceed 20 W m^{-2}. Some megacities, like Shanghai, can have an ~~value of~~ AH flux value as high as 200 W m^{-2}. Except for the urban areas, the AH fluxes are generally less than 5 W m^{-2} in most parts of the YRD region. In particular, in ~~those~~ places where there is no human activity, the AH flux is 0.

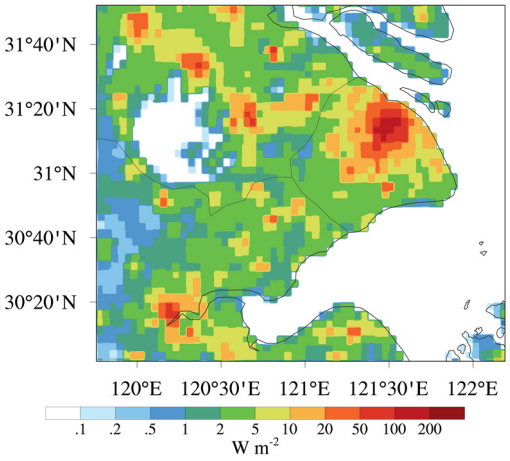

Figure 3. Spatial distribution of anthropogenic heat fluxes in the innermost domain.

2.4 Model setup and experimental designs

In this study, ~~the~~ WRF-Chem version 3.9.1 was~~is~~ applied. The WRF-Chem model is a fully coupled online numerical weather prediction model with chemistry components (Grell et al., 2005), in which ~~,~~ chemical and ~~the~~ meteorological variables use the same coordinates, transport schemes and physics schemes in space and time. ~~The initial and boundary conditions of meteorological fields are from the National Centers for Environmental Prediction (NCEP) global final analysis fields every 6 h with a spatial resolution of 1° × 1°.~~ There are 32 vertical levels extending from the surface to 100 hPa with 12 levels located below 2 km to resolve the boundary layer processes. ~~Furthermore,~~ ~~t~~The domain and options for physical and chemical parameterization schemes are summarized in Table 1. The initial and boundary conditions of meteorological fields are from the National Centers for Environmental Prediction (NCEP) global final analysis fields every 6 h at 1° × 1° resolution. The anthropogenic emissions are provided by the Multiresolution Emission Inventory for China (MEIC) in 2017 with a resolution of 0.25° (http://meicmodel.org/), which includes 10 air pollutants and CO_2 from power, industry, residential, transportation and agriculture sectors. The biogenic emissions are calculated online using the Model of Emissions of Gases and Aerosols from Nature (MEGAN) available in WRF-Chem (Guenther et al., 2006). As our main objective is to explore the response of O_3 to the meteorological changes induced by land use and AH, we use the same surface biogenic emission rates for different land use scenarios (Li et al., 2014, 2017). Further studies will be carried out to quantify the contribution of biogenic volatile organic compounds changed by meteorological conditions to O_3.

Table 1. The domains and major options for WRF-Chem.

Items	Contents
Dimensions (x, y)	(101, 96), (146, 121), (236, 206)
Grid spacing (km)	25, 5, 1
Time step (s)	75
Microphysics	Purdue Lin microphysics scheme (Chen and Sun, 2002)
Longwave radiation	RRTM scheme (Mlawer et al., 1997)
Shortwave radiation	Goddard scheme (Kim and Wang, 2011)
Surface layer	Revised MM5 Monin-Obukhov scheme
Land-surface layer	Noah land-surface model (Chen and Dudhia, 2001)
Planetary boundary layer	YSU scheme (Hong et al., 2006)
Cumulus parameterization	Grell 3D ensemble scheme (Grell and Devenyi, 2002)
Gas-phase chemistry	RADM2 (Stockwelll et al., 1990)
Photolysis scheme	Fast-J photolysis (Fast et al., 2006)
Aerosol module	MADE/SORGAM (Schell et al., 2001)

As shown in Table 2, three numerical experiments are performed. The MODIS_noAH experiment is a control simulation with commonly used settings. Compared with MODIS_noAH, USGS_noAH selects the USGS land use classification at ~~run time~~runtime through the geogrid program. Thus, the difference between the modeling results of MODIS_noAH and USGS_noAH can illustrate the changes caused by land use. ~~As for t~~The impact of AH~~, it~~ can be identified by comparing the modeling results of MODIS_AH and MODIS_noAH because AH is only added in MODIS_AH. To exclude the uncertainty conceivably caused by different configurations, all three simulations use the same emission inventory, physical and chemical parameterization schemes (Table 1), running from 00:00 UTC 21 May to 00:00 UTC 4 June 2017 with the first 88 h as spin-up time.

Table 2. The three numerical experiments.

Scenario	Land use classification	Whether to add AH
MODIS_noAH	MODIS-based	No
USGS_noAH	USGS	No
MODIS_AH	MODIS-based	Yes

2.5 Model evaluation

To verify the model performance, the simulation results in the innermost domain, including O_3 concentration, T_2, RH, WS_{10} and WD_{10} are examined against the surface observations described in Sect. 2.1. The statistical metrics, including the mean bias (MB), root mean square error (RMSE) and correlation coefficient (COR), are also calculated. They are defined as follows:

$$MB = \frac{1}{N}\sum_{i=1}^{N}(S_i - O_i), \quad (1)$$

$$RMSE = \sqrt{\frac{1}{N}\sum_{i=1}^{N}(S_i - O_i)^2}, \quad (2)$$

$$COR = \frac{\sum_{i=1}^{N}(S_i - \bar{S})(O_i - \bar{O})}{\sqrt{\sum_{i=1}^{N}(S_i - \bar{S})^2}\sqrt{\sum_{i=1}^{N}(O_i - \bar{O})^2}}, \quad (3)$$

where S_i and O_i are the simulations and observations, respectively. N is the total amount of valid data, and $\bar{S}$ and $\bar{O}$ represent the average of simulations and observations, respectively. Generally, the model performance is acceptable if the values of *MB* and *RMSE* are close to 0, and that of *COR* is close to 1 (Xie et al., 2016a, b; Zhan et al., 2020).

3 Results and discussions

3.1 Regional O_3 pollution episodes in the YRD

On cloudless sunny days, regional O_3 pollution episodes occur frequently in the YRD (Gao et al.,~~l.,~~ 2020; Zhan et al., 2021), affecting~~which can affect~~ an area of~~ up to~~ 3.5 million square kilometers and harming more than 200 million people. ~~The regional~~Regional O_3 pollution is generally defined as when more than half of the 26 typical cities in the YRD fail to meet the national O_3 standard (~~In~~ in China, the national ambient air quality standard for MDA8 O_3 is 160 μg m^{-3}).

Based on the surface O_3 observations, we sort out all regional O_3 pollution episodes and the corresponding weather patterns from 2015 to 2019 (Table S1). There were 20, 19, 34, 28 and 30 regional O_3 pollution cases in the YRD from 2015 to 2019, respectively. These cases mainly occurred in April to October of each year, and were usually related to high pressure, uniform pressure ~~field~~ fields and typhoon activity.

Figure 4 further displays the monthly distribution of meteorological factors during the daytime (from 8:00 to 20:00 local time) when regional O_3 pollution occurs in the YRD. All the variables show significant monthly variations. The highest (lowest) temperature is found in July (April), and the relative humidity is highest in June. As for the cloud cover, the sky is covered with fewer clouds in October than in other months. In addition, southeast winds ~~prevails~~ prevail in the YRD from April to October under the influence of the monsoon climate. The correlation coefficients between temperature, relative humidity, cloud cover, wind speed and MDA8 O_3 are 0.12, -0.34, -0.15 and 0.04, respectively. Therefore, O_3 pollution episodes tend to occur on days characterized by high temperature, low relative humidity, cloudless sky and light wind (the weak correlation between wind speed and MDA8 O_3 is due to the small change in light wind). More specifically, on days when the temperature exceeds 20 ℃ (Figure 4b), the relative humidity is less than 80% (Figure 4c), the cloud cover is less than 5 okta (Figure 4d), and the wind speed is less than 3 m s^{-1} (Figure 4e) in the YRD. On the other hand, local circulations are clearest when in absence of clouds, radiative heating is strongest and wind is weakest. In this case, local circulation will~~can~~ inevitably have an impact on the ~~evolution~~ distribution of O_3.

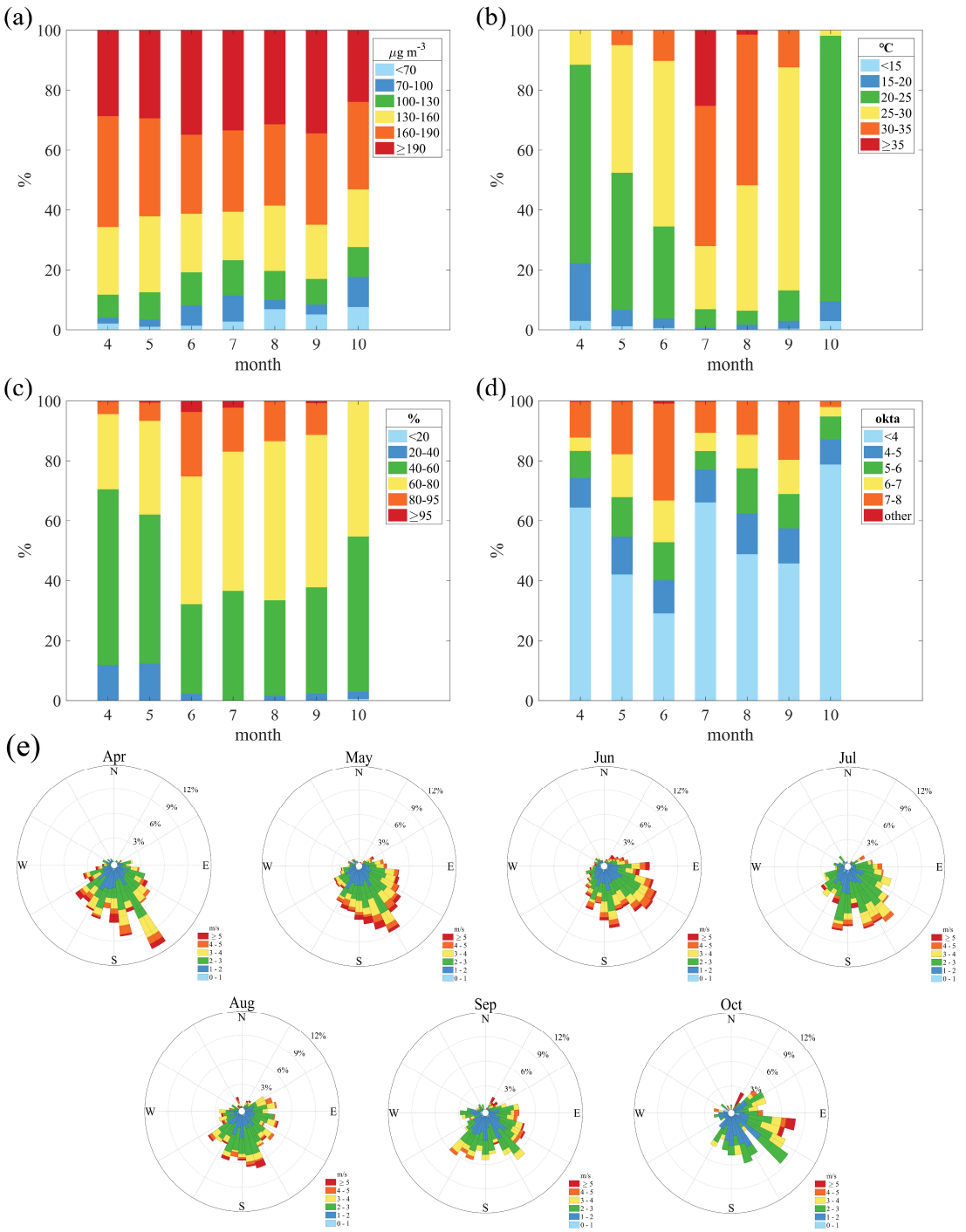

Figure 4. The monthly distributions of (a) MDA8 O_3, (b) temperature, (c) relative humidity, (d) cloud cover, and (e) wind speed and direction during the daytime (8:00 to 20:00 LT) when regional O_3 pollution occurs in the YRD.

3.2 Case selection

3.2.1 Case for O_3 pollution episode

For simplicity but without loss of generality, the longest-lasting regional O_3 pollution episode is selected to investigate the impacts of land use and AH on meteorology and O_3 in the YRD. This 10-day regional O_3 pollution episode occurred from 25 May to 3 June ~~in~~ 2017 (Table S1). Dominated by high pressure/uniform pressure fields (Figure S1), high O_3 concentrations are accompanied by high air temperature, low relative humidity, light wind and shallow cloud cover during this smog episode. An average of 18 out of the 26 cities experienced O_3 pollution every day with MDA8 O_3 concentrations ranging~~ranged~~ from 80.0 to 269.0 μg m^{-3} in the YRD. With regard to the meteorological factors, T_2 ranged from 12.9 to 33.5 ℃, with an average of 26.4 ℃; RH ranged from 26.6 to 99.4~~-~~%, with an average of 58.6~~-~~%; WS_{10} ranged from 0.5 to 10.8 m s^{-1}, with an average of 2.8 m s^{-1}; CC ranged from 0 to 8.4 okta, with an average of 4.2 okta (Table 3). The values of these meteorological factors meet the standards in the previous section ~~,~~ and can cover both the whole YRD and the central YRD region (the innermost domain). Therefore, this O_3 pollution episode not only meets the requirements of high O_3 ~~concentration~~ concentrations but also calm~~lam~~ weather conditions. ~~And t~~The long duration also provides relatively universal results.

Table 3. Mean, minimum and maximum of MDA8 O_3, T_2, RH, WS_{10} and CC during the daytime from 25 May to 3 June 2017.

	The YRD region			The central YRD region		
	Mean	Minimum	Maximum	Mean	Minimum	Maximum
MDA8 O_3 (μg m^{-3})	182.1	80.0	269.0	177.8	118.0	251.0
T_2 (℃)	26.4	12.9	33.5	26.7	21.4	29.8
RH (%)	58.6	26.6	99.4	52.9	33.8	73.7
WS_{10} (m s^{-1})	2.8	0.5	10.8	3.6	1.6	6.0
CC (okta)	4.2	0	8.4	3.3	0	7.4

3.2.2 Evaluation of model performance

To evaluate the model performance, the simulation results in the innermost domain are validated by comparing with the observational data. Table 4 presents the statistical metrics in meteorological factors. Figure 5 further illustrates the time series of these meteorological factors and their modeling results. T_2 is reasonably well simulated as the CORs (the mean of all the sites) are 0.87, 0.86 and 0.86 in MODIS_noAH, USGS_noAH and MODIS_AH, respectively. The small negative MBs at all sites suggest that our simulations underestimate T_2 to some extent,

although~~though~~ this light underestimation is acceptable because of the small RMSEs (2.3, 3.1 and 2.3 ℃). The MBs for T_2 in USGS_noAH, MODIS_noAH and MODIS_AH are -2.4, -1.0, and -0.8 ℃~~, indicting an improvement in temperature when new land use and AH are taken into account~~. The smaller RMSEs and MBs indicate that the T_2 simulation is improved when new land use and AH are taken into account, which may be related to the improved latent and sensible heat fluxes in models (De Meij and Vinuesa, 2014). The improvement ~~is~~ can also be confirmed by Figure 5a. With respect to RH, the CORs are 0.82, 0.75 and 0.83 in~~for~~ MODIS_noAH, USGS_noAH and MODIS_AH, respectively. Thus, all three simulations can ~~well~~ capture the diurnal variation of RH well~~,~~ but have different performances at~~on~~ different sites~~ (Figure 5b)~~. In USGS_noAH, RH is overestimated at all sites, especially the Pudong site with an~~the~~ MB of~~is~~ 11.2%. While RH is overestimated at the two coastal sites (Pudong and Shanghai) but underestimated at other two sites (Hongqiao and Xiaoshan) in MODIS_noAH and MODIS_AH. Moreover, USGS_noAH has the highest RMSEs of RH (16.3%), followed by MODIS_AH (12.4%) and MODIS_noAH (12.1%). Among the three experiments, the simulation result of RH in USGS_noAH is the worst (Figure 5b). As for WS_{10}, the modeling values are slightly overestimated at all sites in all three simulations. The overestimation of WS_{10} may partly be attributed to the unresolved terrain features by the default surface drag parameterization causing an overestimation of wind speed especially at low values (Jimenez and Dudhia, 2012). In particular, WS_{10} in USGS_noAH is the most overestimated, followed by MODIS_AH and MODIS_noAH with~~the~~ MBs of~~are~~ 1.2, 1.0 and 0.8 m s^{-1}, respectively. In addition, high MBs of WS_{10} ~~are corresponding~~correspond to high RMSEs (1.9, 1.8 and 1.7 m s^{-1}) in our simulations. The MODIS-based land cover shows a larger urban fraction, and thereby leads to more friction and higher roughness than the USGS dataset. In this case, the overestimation of WS_{10} is somewhat neutralized to fit the observations. In terms of WD_{10}, the model captures well the shift in wind direction during the study period (Figure 5d). ~~Thus, our modeling results of wind speed and direction basically reflect the characteristics of wind fields.~~ In summary, both the statistical metrics in Table 4 and the time series in Figure 5 indicate that all three numerical experiments can capture the major changes in~~ about~~ meteorological factors during this O_3 pollution episode. Nevertheless, updating the land use and adding AH can ~~somewhat~~ reduce the underestimation of T_2 and the overestimation of RH and WS_{10} in models. Benefitting from the development of computers, numerical models grow more complex, and the resolution requirements are higher. This puts

forward demands on many basic parameters. An updated land cover dataset, like the GLC, contains useful information and can improve the model results (Chen et al., 2016; Wang et al., 2018). Some factors that are generally ignored in models, like the AH fluxes, should also be estimated and evaluated.–

Table 4. Statistical metrics in meteorological variables between observations and simulations.

Variables	Site		MODIS_noAH				USGS_noAH				MODIS_AH			
		$\bar{O}$[a]	$\bar{S}$[b]	MB[c]	RMSE[d]	COR[e]	$\bar{S}$	MB	RMSE	COR	$\bar{S}$	MB	RMSE	COR
T_2	Pd	23.2	21.5	-1.7	2.4	0.89	20.7	-2.5	3.8	0.70	21.5	-1.7	2.4	0.89
(°C)	Sh	24.6	23.9	-0.7	2.2	0.87	22.5	-2.1	2.7	0.90	24.2	-0.5	2.3	0.84
	Hq	25.3	24.4	-0.9	2.0	0.89	22.7	-2.6	3.0	0.95	24.8	-0.5	1.9	0.89
	Xs	25.9	25.1	-0.8	2.4	0.85	23.8	-2.2	2.8	0.91	25.5	-0.4	2.4	0.83
RH	Pd	69.1	77.7	8.6	13.5	0.81	86.2	17.2	23.4	0.45	77.7	8.7	13.3	0.83
(%)	Sh	59.3	60.6	1.3	11.7	0.81	71.1	11.8	16.1	0.81	59.4	0.1	12.4	0.78
	Hq	59.5	57.7	-1.8	9.8	0.88	70.6	11.1	14.5	0.89	56.2	-3.3	9.8	0.89
	Xs	60.6	55.4	-5.2	13.5	0.79	65.3	4.8	11.3	0.86	53.5	-7.1	14.1	0.80
WS_{10}	Pd	4.1	4.1	0.0	1.4	0.47	5.5	1.3	2.1	0.35	4.2	0.1	1.3	0.51
($m\ s^{-1}$)	Sh	2.5	4.2	1.7	2.2	0.36	4.5	2.0	2.4	0.54	4.3	1.9	2.3	0.35
	Hq	3.7	3.9	0.2	1.2	0.54	3.9	0.2	1.2	0.53	4.2	0.5	1.3	0.50
	Xs	2.3	3.6	1.3	2.0	0.26	3.4	1.1	1.8	0.30	3.8	1.5	2.1	0.24
WD_{10}	Pd	160.4	136.1	-26.2	78.7	0.42	148.1	-14.3	55.1	0.72	137.3	-24.7	77.5	0.42
(°)	Sh	141.6	146.4	4.8	66.4	0.60	141.7	0.1	63.9	0.59	142.6	1.0	69.9	0.56
	Hq	159.7	140.2	-23.4	80.2	0.46	153.1	-10.6	74.9	0.52	142.8	-20.4	91.8	0.29
	Xs	188.6	160.2	-28.4	99.5	0.48	161.4	-27.3	109.6	0.35	152.0	-36.6	109.9	0.38

[a] $\bar{O}$ and [b] $\bar{S}$ indicate the average of observations and simulations, respectively. [c] MB indicates the mean bias, [d] RMSE indicates the root mean square error and [e] COR indicates the correlation coefficient, with ~~statistically significant at 99% confident~~statistical significance at the 99% confidence level.

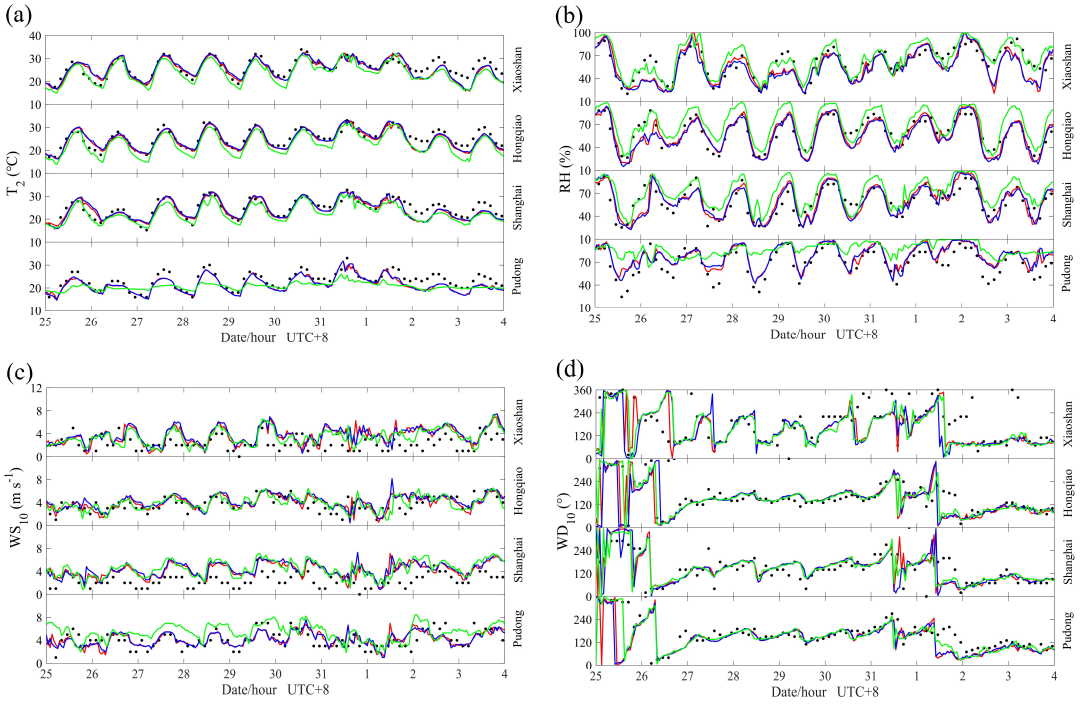

Figure 5. Time series of (a) T_2, (b) RH, (c) WS_{10} and (d) WD_{10} for observations and simulations at different weather stations. The black dots are the surface observations. The simulation results of MODIS_noAH, USGS_noAH and MODIS_AH are shown in red, green and blue lines, respectively.

Table 5 lists the statistical metrics in O_3, and Figure 6 gives the hourly variations in~~of~~ O_3 for observations and simulations in different cities. With high CORs (the CORs are 0.80, 0.81 and 0.80 in MODIS_noAH, USGS_noAH and MODIS_AH, respectively), all three simulations well reproduce the diurnal variation in~~of~~ O_3, which is that O_3 concentration reaches its maximum in the afternoon and ~~gradually~~ decreases to its minimum in the morning. The magnitudes of O_3 modeling results are reasonable (Figure 6), but the peak and valley values of O_3 simulations ~~are~~ sometimes differ from the observations, especially the peak values, like Huzhou. Considering the relatively low MBs (6.9, -1.6 and 9.0 μg m^{-3}) and RMSEs (49.3, 46.2 and 49.0 μg m^{-3}), the modeling results of O_3 are generally reasonable and acceptable.

Table 5. Statistical metrics in O_3 (μg m^{-3}) between observations and simulations.

Case	Index	City						
		CZ	WX	SZ	SH	HZ1	JX	HZ

	$\bar{O}$	89.7	141.8	121.7	112.8	95.8	113.2	104.8
MODIS_noAH	$\bar{S}$	123.2	117.6	116.2	103.4	128.1	112.5	127.5
	MB	33.3	-24.2	-5.6	-9.1	32.1	-0.6	22.7
	RMSE	53.8	49.1	42.8	36.4	59.9	44.4	58.6
	COR	0.85	0.83	0.82	0.80	0.83	0.78	0.71
USGS_noAH	$\bar{S}$	108.1	106.8	107.1	93.8	118.6	111.0	122.5
	MB	18.5	-35.0	-14.7	-18.9	23.0	-2.0	18.0
	RMSE	43.5	56.0	44.7	37.7	50.1	41.1	50.0
	COR	0.83	0.81	0.80	0.81	0.82	0.80	0.77
MODIS_AH	$\bar{S}$	124.5	119.8	119.1	108.0	130.3	113.7	127.8
	MB	34.7	-21.9	-2.7	-4.6	34.3	0.6	23.0
	RMSE	53.5	47.3	42.4	37.4	59.4	44.7	58.2
	COR	0.84	0.83	0.81	0.80	0.82	0.78	0.71

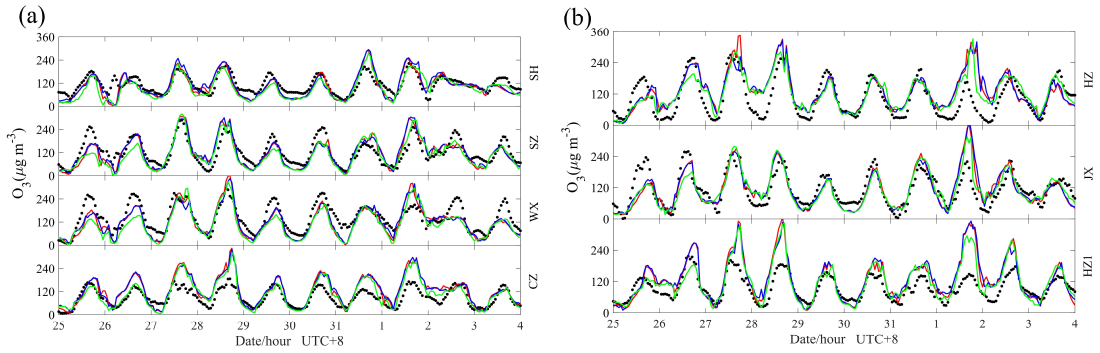

Figure 6. Same as Figure 5, but for O_3.

Above all, the WRF-Chem model using our configuration has a good capability in simulating the meteorological factors and O_3 over the studied region. In addition, it is noteworthy that the object of inter-comparisons between the three numerical experiments are not to determine which setting is the most skillful in reproducing the observations. Rather, it is to diagnose and understand the changes induced by land use and AH, and the response of O_3 to these changes.

3.3 Overall behaviors of O_3 and local circulations

Based on the results of the control simulation (MODIS_noAH), we first give an overall behavior of O_3 and local circulations during the study period. Then the changes induced by land use and AH are discussed via inter-comparisons between different numerical experiments~~scenarios simulations~~. Therefore~~Thereby~~, only difference plots between USGS_noAH/MODIS_AH and MODIS_noAH are shown in this paper, and the corresponding original plots for

USGS_noAH/MODIS_AH can be found in the supplementary materials (Figure S2-7).

3.3.1 Spatiotemporal variations of O_3

As shownshow in Figure 7, O_3 concentration began to rise around 8:00 local time (LT = UTC + 8 h), and became noticeable after only 3 hours (Figure 7a and h). During this stage, the nocturnal residual layer vanished due to the development of the convective boundary layer (Figure 8). The O_3-rich air mass in the residual layer was mixed with the O_3-poor air mass on the ground, which enhanced the surface O_3 in the morning (Hu et al., 2018). Around 11:00 LT, the a convective boundary layer was established (Figure 8), and high O_3 produced by photochemical reactions appeared over the central YRD and persisted until 18:00 LT (Figure 7b and c). After sunset, surface O_3 concentration generally decreased due to nitrogen oxide (NO) titration, and reached its minimum in the early morning (Figure 7f and g). In general, O_3 has a typical diurnal variation with high concentrationsconcentration in the daytime and low concentrationsconcentration at night. This is consistent with the observations in Figure 6, and this rule of O_3 can be applied to most parts of the world. Therefore, the situation during the daytime (we select 11:00, 14:00, 17:00 and 20:00 LT in this study) should be paid attention to when it comes toconsidered in regard to O_3 pollution.

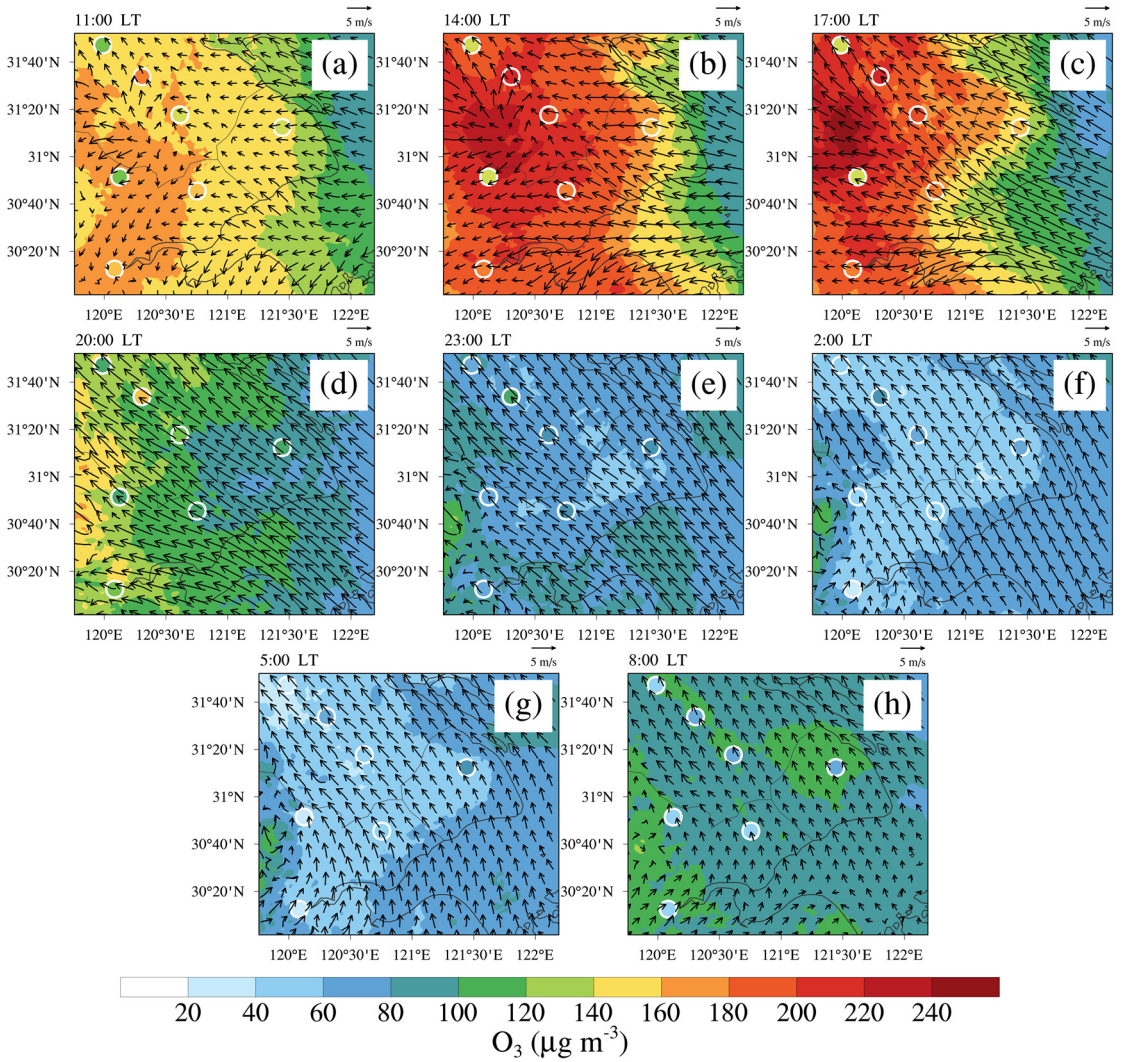

389

390 **Figure 7.** Horizontal distributions of O_3 and wind at the lowest model level in MODIS_noAH. (a),

391 (b), (c) and (d) show~~are~~ the results at 11:00, 14:00, 17:00 and 20:00 LT, referring to the daytime. (e),

392 (f), (g) and (h) show~~are~~ the results at 23:00, 2:00, 5:00 and 8:00 LT, referring to the night. The

393 observations in different cities are overlaid using colored circles. To obtain universal features, all

394 results are the average of the study period, and the same for the subsequent results.

395

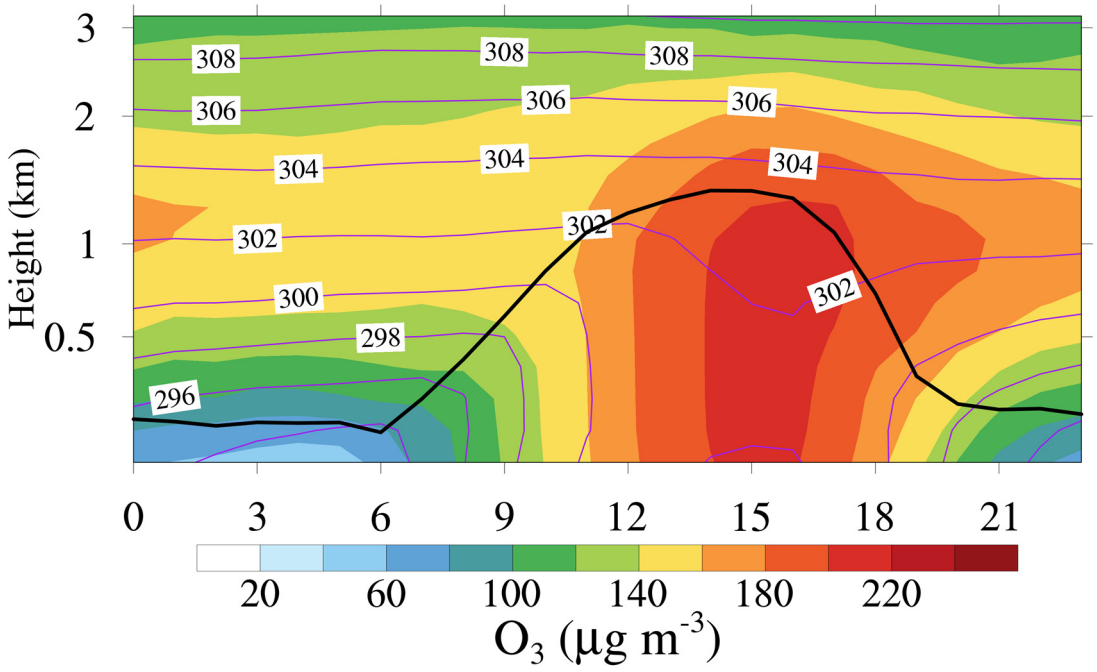

Figure 8. Temporal-vertical distribution of O_3 and potential temperature covering the CZ, WX, SZ, SH, HZ1, JX and HZ over the innermost domain in~~of~~ MODIS_noAH.

3.3.2 The s~~S~~ea and lake breezes

As shown in Figure 7a and b, high O_3 ~~concentration~~ concentrations in the central YRD tended to appear in the converging airflows associated with the sea breeze, the lake breeze and the background southeast wind (Figure 4e). The sea breeze and the background southeast wind were usually in the same direction, and thereby sea breeze affected a wide area and lasted a long time. The sea breeze was obvious around 14:00 LT, ~~and~~ matured around 17:00 LT, and continuously transported high O_3 from coastal to inland areas during this period (Figure 7b-d). Compared with the sea breeze, the lake breeze had a much smaller influencing area and a shorter duration. Around 11:00 LT, the lake breeze was established. It reached its maximum intensity around 14:00 LT, ~~,~~and then disappeared sharply due to the predominant southeast wind (Figure 7b and c). Both the sea and the lake breezes are the typical local circulations in the YRD, and~~which~~ play~~s~~ important roles in the horizontal distributions of O_3 over this region.

Since the coastline is generally north-south (Figure 1b), the cross sections along blue line AB (east-west) depicted in Figure 2a are illustrated to show representative examples of the vertical structure of the sea breeze (Figure 9a-c). By 11:00 LT, the sea breeze below 500 m had already

developed. The sea breeze front was found in front of Shanghai (~121.6°E), with a height of 1.5 km (Figure 9a). Around 14:00 LT, the speed of sea breeze increased, ~~which exceeded~~exceeding 5 m s^{-1}. The sea breeze front moved inland for a distance of 20-30 km (~121.4°E), and was elevated to ~2 km (Figure 9b). Around 17:00 LT, the~~strong~~ sea breeze ~~swept across the central YRD~~matured, reducing the O_3 concentration near the surface in Shanghai. However, ~~But~~ the O_3 in the mixed layer still maintained a high level, which may result in an O_3-rich reservoir forming in the nocturnal residual layer (Figure 9c). The penetration of the sea breeze front and its effect on surface O_3 are also observed in other coastal regions, such as Taiwan (Lin et al., 2007), the Athens basin (Mavrakou et al., 2012) and Paulo (Freitas et al., 2007).

As for the lake breeze, since the lake is inside the land, the lake breeze has different directions. Thus, the cross sections along green line CD (south-north) and black line EF (east-west) in Figure 2a are given. ~~since the lake is usually inside the land so that the lake breeze can have different directions.~~ The lake breeze was established by 11:00 LT (Figure 9d and g) although it was shallow at that time. Around 14:00 LT, the lake breeze strengthened. The extension of the lake breeze circulation zone can ~~even~~ reach up to 2 km in the vertical dimension (Figure 9e). The offshore flow of the lake breeze circulation (~2 m s^{-1}) transported high O_3 concentrations from the urban areas to the lake, while the onshore flow blew the O_3 back to urban areas (Figure 9e and h). Thus, the net effect of the lake breeze is to accelerate the vertical mixing of O_3 in the boundary layer, resulting in high surface O_3 in the lakeside cities. This was also reported in other lakeside cities, such as the Lake Michigan (Lennartson and Schwartz, 2002), the Great Lakes (Sills et al., 2011) and the Great Salt Lake (Blaylock et al., 2017). By 17:00 LT, the lake breeze disappeared.

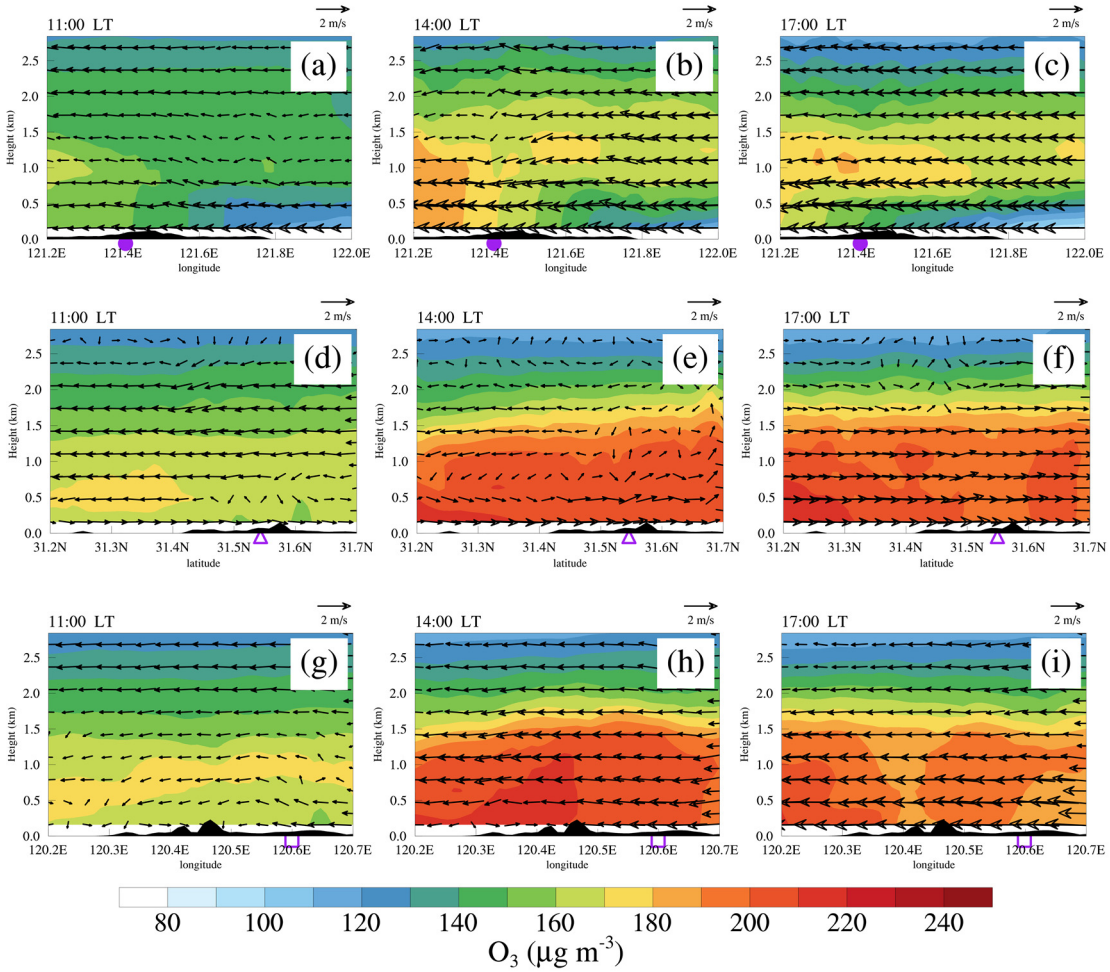

Figure 9. Vertical cross sections of O_3 and wind for the sea breeze at (a) 11:00, (b) 14:00 and (c) 17:00 LT along blue line AB in Figure 2a. (d), (e) and (f) are the same as (a), (b) and (c), respectively, but for the lake breeze along green line CD in Figure 2a. (g), (h) and (i) are also the same as (a), (b) and (c), respectively, but for the lake breeze along black line EF in Figure 2a. The purple dots, triangles and rectangles represent the locations of Shanghai, Wuxi and Suzhou, respectively. The black shaded areas represent the terrain, and the terrain is~~has been~~ multiplied by a factor of 10 when plotting.

3.4 Impacts of land use on meteorology and O_3

3.4.1 The changes in horizontal direction

Figure 10 presents the spatial differences of the main factors (T_2, PBLH, WS_{10} and O_3) between MODIS_noAH and USGS_noAH. Land use changes via urban expansion can enhance surface heating through upward sensible heat fluxes so that T_2 will increase. As shown in Figure 10a-d, the

spatial pattern of the remarkable warming effect for T_2 was consistent with the urban ~~-~~fraction change associated with ~~the~~ urbanization (Figure 2a and b), which is the positive temperature anomaly that mainly ~~–~~appeared in cities and their surrounding areas. In megacities like Shanghai, T_2 increased by even 3 ℃. The change in PBLH was similar to that in T_2 because the warming up of T_2 was conducive~~conductive~~ to ~~the~~ vertical movement in the boundary layer, which increased the PBLH (Figure 10e-h). The maximum positive change of PBLH can reach up to 500 m at noon but down to 100 m after sunset. With regard to ~~the~~ WS_{10}, it decreased in ~~the~~ MODIS_noAH (Figure 10i-l), with a maximum decrease up to 1.5 m s^{-1} in Hangzhou around 17:00 LT. This is because the roughness of cities and forest is larger than that of cropland (Figure 2a and b). Apart from the abovementioned meteorological factors, urban expansion also increased the surface O_3 concentration (Figure 10m-p). The largest increment of O_3 appeared in the afternoon, with a value of 20 μg m^{-3} around 17:00 LT in Changzhou. In addition to these results, it is noteworthy that there were confusing "false" changes at the junction of land and sea/lake, especially for meteorological factors, such as T_2 and WS_{10}. This was caused by the different treatments~~treatment~~ of the MODIS-based and USGS land use classifications at the boundary conditions of land versus water instead of urban expansion.

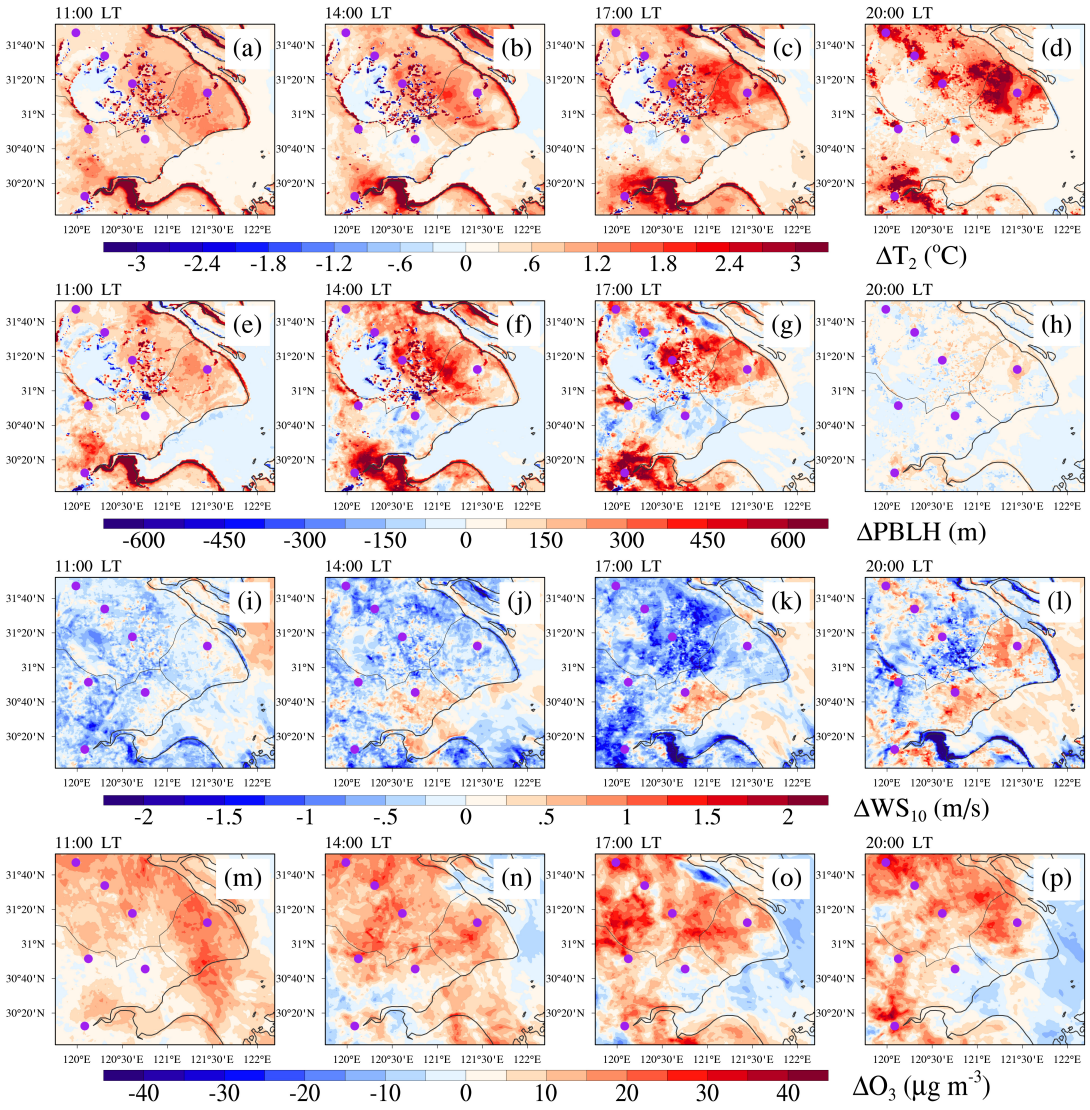

Figure 10. Horizontal distributions of the differences of (a-d) T_2, (e-h) PBLH, (i-l) WS_{10} and (m-p) O_3 ~~differences~~ between MODIS_noAH and USGS_noAH (MODIS_noAH – USGS_noAH) during the daytime. The purple dots represent the locations of cities in the innermost domain.

3.4.2 The changes in vertical direction

Urban expansion alters not only ~~alters~~ the meteorological factors~~,~~ but also the local circulations. As shown in Figure 11a-c, the sea breeze below 500 m increased by ~1 m s^{-1} due to the enhanced temperature contrast between the land and the sea induced by the expansion of Shanghai. During the advance of the sea breeze front inland, the updraft induced by the sea breeze front promoted the vertical mixing of O_3, elevating the surface O_3 concentration in Shanghai (Figure 11a and b). When the sea breeze matured around 17:00 LT, its transport effect reduced the surface O_3 concentration of the coastal cities (Figure 9c). However, this "transport effect" was weakened because the sea breeze

near the surface was slowed affected by the rough urban surface. Finally, surface O_3 of ~10 μg m^{-3} was left compared to the scenario without cities. In contrast to the onshore flow, the offshore flow transported O_3 ~~high concentration of O_3~~ to the sea, which may be an important source of O_3 in the nocturnal residual layer. Influenced by the strong background southeast wind, the offshore flow was imperceptible during the daytime (Figure 9), but it was~~can be~~ enhanced by urban expansion (Figure 11c).

As for the lake breeze, it was also enhanced by ~1 m s^{-1} because of the larger temperature contrast resulting from the expansion of lakeside cities (Figure 11e and h). ~~What's more~~Moreover, the life of the lake breeze was extended to 17:00 LT (Figure 11f and i). Since the lake breeze circulation was conducive to the vertical mixing of O_3 in the boundary layer~~, and its onshore flow transported high concentration of O_3 from the lake to the city~~ (Sect. 3.3.2), the O_3 concentration will increase in the lakeside cities, with a maximum of 30 μg m^{-3} in Wuxi at 14:00 LT.

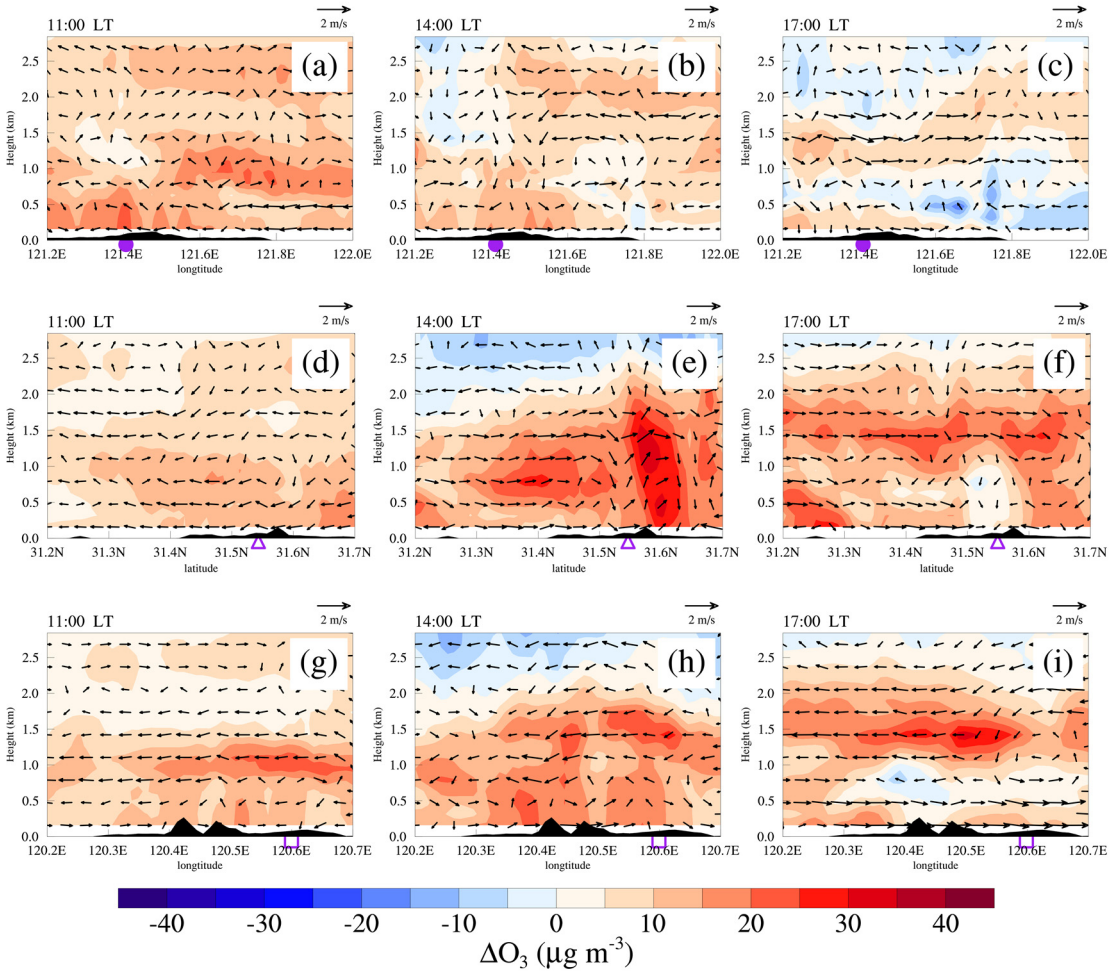

Figure 11. Same as Figure 9, but for the differences between MODIS_noAH and USGS_noAH (MODIS_noAH – USGS_noAH).

3.4.3 The mechanism of land use modulating O_3

Changing land use from USGS to MODIS leads to an increase in T_2 by a maximum of 3 ℃, an increase in PBLH by a maximum of 500 m and a decrease in WS_{10} by a maximum of 1.5 m s^{-1} in the YRD, which is comparable to those in the BTH region (Yu et al., 2012), the PRD region (Li et al., 2014) and the National Capital Region of India (Sati and Mohan, 2017). These changes are particularly evident in and around cities as the largest~~biggest~~ change in land use is ~~related to urban expansion~~urban surface fractions. ~~The el~~Elevated air temperature is conducive to the photochemical production of O_3, and the well-developed convective boundary layer favors the vertical mixing of O_3. These changes in meteorological factors_ —eventually increase the surface O_3 concentration by a maximum of 20 μg m^{-3} in the YRD. Furthermore, local circulations, including the sea and the lake breezes, are also influenced by urban expansion, which further alters O_3 in the vertical direction. For ~~the~~ coastal cities, like Shanghai, the larger temperature contrast caused by cities enhances the sea breeze ~~below 500 m~~. As the sea breeze front moves inland, it enhances upward movement, which is conducive~~conductive~~ to the mixing of O_3 in the boundary layer. However, the movement of the sea breeze is slowed due to the rough urban surface after the sea breeze matures. The removal of O_3 via the sea breeze near the surface is then weakened. ~~The~~ A similar response of the sea breeze to cities as well as its impact on O_3 has also been ~~also~~ reported in the PRD region (You et al., 2019) and Paulo (Freitas et al., 2007). For the lakeside cities, like Wuxi and Suzhou, the lifetime of ~~the~~ lake breezes is extended to the afternoon due to the expansion of cities. The offshore flow of the lake breeze transports high O_3 ~~concentration~~ concentrations in the middle of the boundary layer from the land to the lake, while the onshore flow brings the O_3 back to the land, which accelerates the vertical mixing of O_3 and increases the surface O_3. Thus, high surface O_3 usually appears when the lake breeze is established. This was also observed in the Greater Toronto Area (Wentworth et al., 2015) and the Lake Michigan (Abdi-Oskouei et al., 2020).

3.5 Impacts of anthropogenic heat on meteorology and O_3

3.5.1 Horizontal changes

Compared with land use, the changes caused by AH are much smaller (Figure 12). Furthermore, these changes are effective in and around cities as they usually have large AH flux densities~~y~~ (Figure 3). By adding more surface sensible heat into the atmosphere, the AH fluxes leaded to an increase in T_2 of 0.2 ℃ in urban areas, with ~~the~~ a typical value of 0.42 ℃ in Shanghai (Figure 12a-d). Vertical air movement in the boundary layer was then enhanced by the warming of T_2, and the PBLH ~~will increase~~increased as well. According to the simulations, the PBLH increased by ~75 m in the urban areas (Figure 12e-h). Contrary to the decrease in WS_{10} caused by urban expansion, WS_{10} increased by ~0.3 m s^{-1} in the urban areas when AH fluxes were taken into account (Figure 12i-l). This is ascribed to the strengthened urban breeze circulations~~ caused by the AH fluxes~~, which ~~is~~ are conducive to the transmission of momentum from the upper layer to the surface. With regard to surface O_3 concentration, it increased by ~4 μg m^{-3} in the simulation with adding AH. ~~In particular~~What's more, the increases in T_2, PBLH, WS_{10} and O_3 ~~seemed to be~~were clearer after sunset as the solar shortwave radiation disappeared.

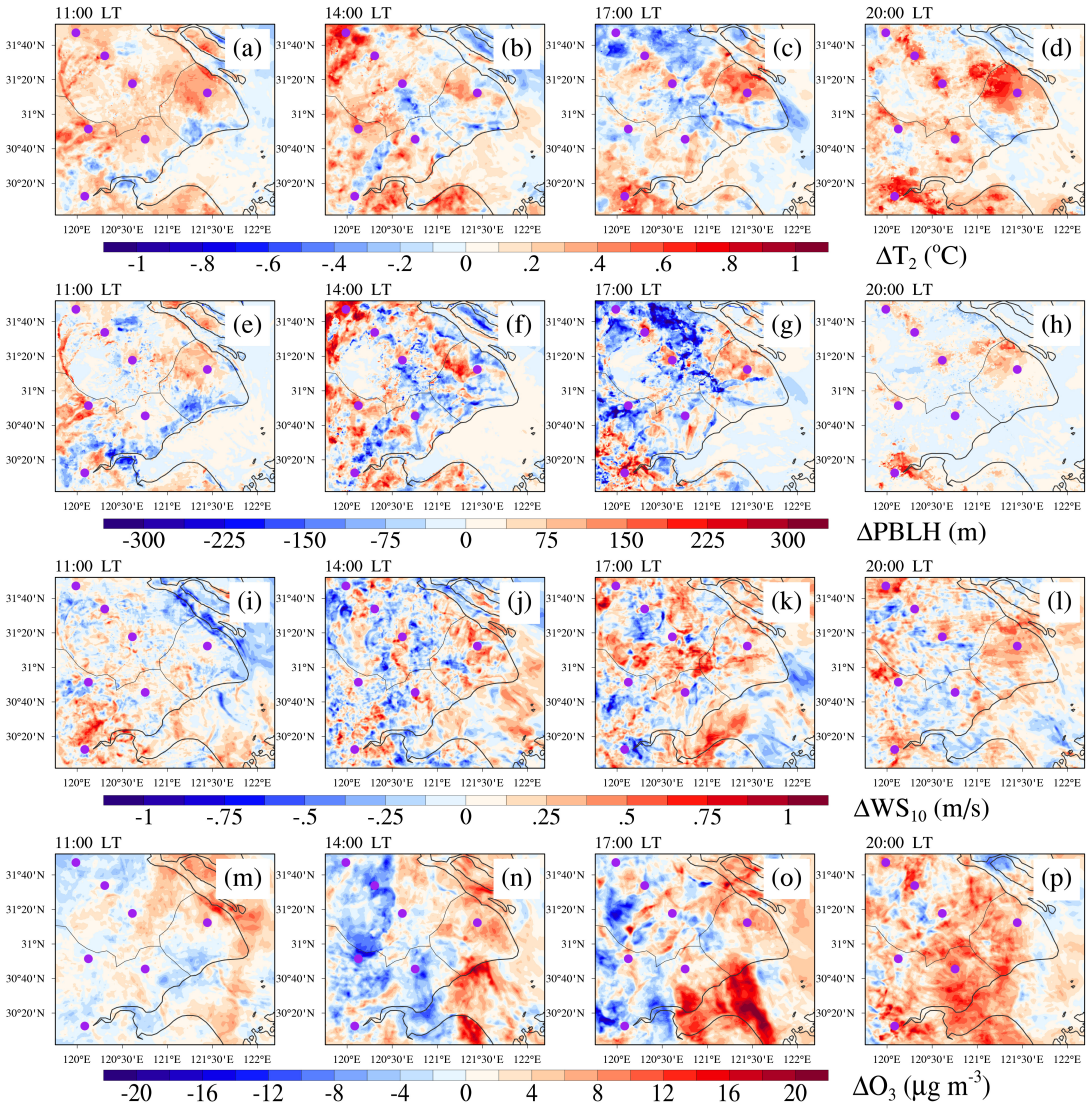

Figure 12. Same as Figure 10, but for the differences between MODIS_AH and MODIS_noAH (MODIS_AH – MODIS_noAH).

3.5.2 Vertical changes

The phenomenon that cities are almost always warmer than their surroundings is widely known as the urban heat island (UHI), and ~~the~~ this ~~difference between the urban and the rural surface energy balance~~urban-rural difference in temperature can further induce the urban heat island circulation (UHIC). ~~It is clearly seen that~~There was an enhanced UHIC driven by AH ~~appeared~~ in ~~the~~ megacity Shanghai around 14:00 LT (Figure 13b). This circulation extended horizontally 20-30 km from the city center to the urban edge, and vertically to ~2 km from the ground to the top of the urban boundary layer, resulting in~~. In this case, there was~~ a small increase (4~6 μg m^{-3}) in surface O_3. However, for the lakeside cities, the enhanced UHIC was not perceptible. ~~And t~~The O_3 concentration

in urban areas was reduced on average, with a maximum of 16 μg m^{-3} in Wuxi around 14:00 LT (Figure 13e). The decrease in O_3 may be related to the increased wind (Figure 12i-k), which was beneficial to the diffusion and dilution of O_3. Furthermore, AH has a limited effect on the sea and the lake breezes as it cannot affect any branch of the two as significantly as ~~the~~ urban expansion.

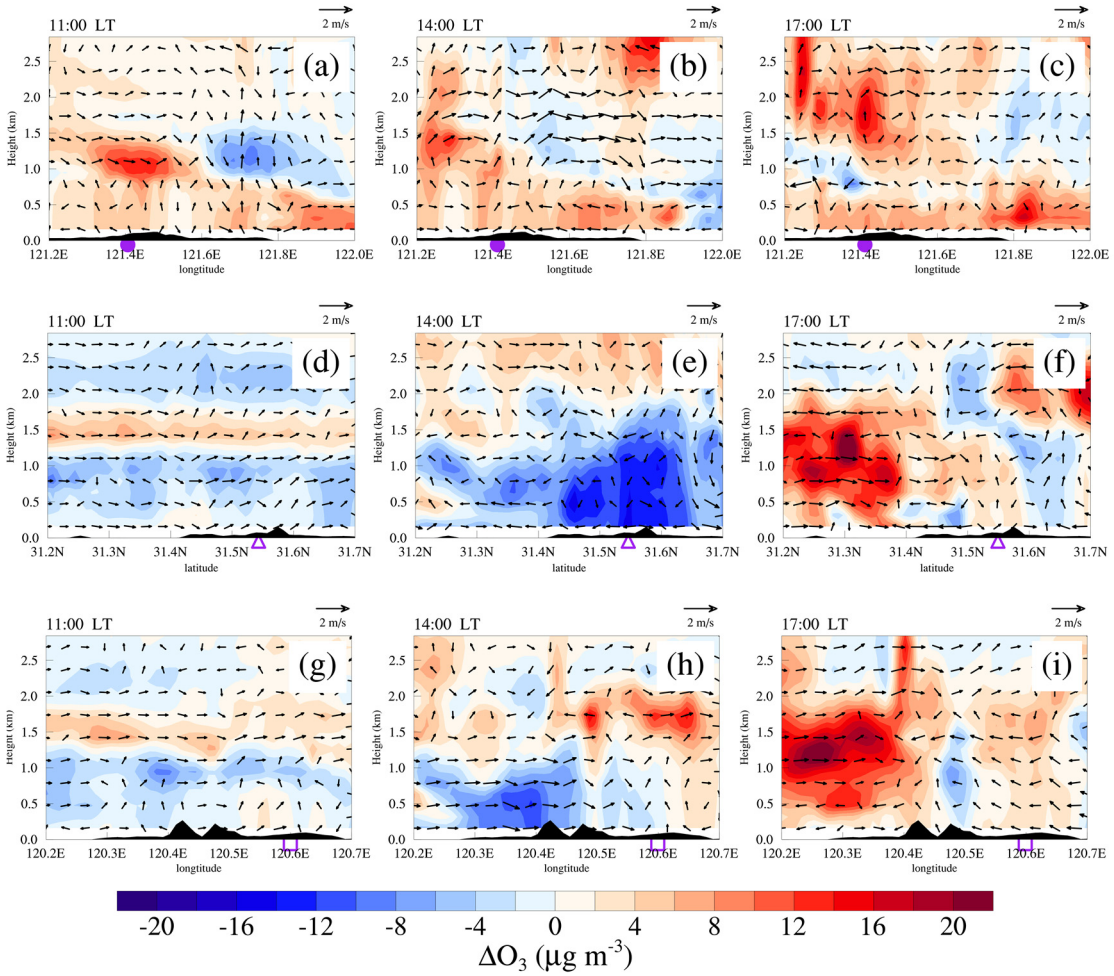

Figure 13. Same as Figure 9, but for the differences between MODIS_AH and MODIS_noAH (MODIS_AH – MODIS_noAH).

3.5.3 The mechanism of anthropogenic heat modulating O_3

AH and land use play different roles in meteorology and O_3. AH allows the atmosphere to reserve more energy via the additional sensible heat fluxes, which increases T_2 by ~0.2 ℃. Higher temperature induces stronger upward air movement to the development of the convective boundary layer, rising the PBLH by ~75 m. In the convective boundary layer, the atmosphere is associated

with turbulent motions, and is unstable. Together with the enhanced urban breeze caused by AH, WS_{10} increases by ~0.3 m s^{-1}. These findings are comparable to the values estimated in other cities all around the world, such as Philadelphia in the United States (Fan and Sailor, 2005), Winnipeg in Canada (Ferguson and Woodbury, 2007) and Berlin in GermanyGerman (Menberg et al., 2013). These changes in meteorological factors eventually lead to an increase in surface O_3 by ~4 μg m^{-3}. It is noteworthy that the effects of AH are usually clearer at night in urban areas. In addition, althoughthough AH plays an important role in urban breeze circulations, it may not be powerful enough to affectt the –local circulations such as the sea and the lake breezes.

4 Summary and conclusions

Land use change via urban expansion and the increase of AH release are important manifestations of urbanization. They can alter the regional meteorology, and thereby affect O_3 concentrations in and around cities. In this study, the YRD region, a highly urbanized coastal area with severesever O_3 pollution, is selected to investigatediscuss this issue. Firstly, the basic characteristics of O_3 pollution in the YRD are providedinvestigated based on the surface observations. Secondly, a representative case is selected forto further study using the WRF-Chem model, and the model performance is evaluated by comparing with the observations. Finally, the response of O_3 to changes in meteorology caused by urban expansionland use and AH are discussed via the model inter-comparisons. The main findings are listed as below:

(1) Regional O_3 pollution occurredfrequently in the YRD (~26 times per year) from 2015 to 2019. These O_3 pollution episodes mainly occur in calm conditions characterized by high temperature (over 20 °C), low relative humidity (less than 80%), light wind (less than 3 m s^{-1}) and shallow cloud cover (less than 5 okta). In this case, the sea and the lake breezes tend to develop and have an important impact on the distribution of O_3 in thethis region YRD.

(2) By updating the land use dataset from USGS to MODIS, we find an increase in T_2 by a maximum of 3 °C, an increase in PBLH by a maximum of 500 m and a decrease in WS_{10} by a maximum of 1.5 m s^{-1} in the YRD. The higher temperature and PBLH elevate the surface O_3 concentration by a maximum of 20 μg m^{-3} via the stronger photochemical reactions and vertical mixing processes. These changes are mainly attributedApart from meteorological factors, the sea and the lake breezes are also modified by urban expansion associated with urbanization. Tto urban

~~expansion associated with urbanization. Furthermore, t~~he sea breeze is enhanced due to the expansion of coastal cities. Nevertheless, further progression inland of the sea breeze ~~in the afternoon is~~can be stalled in the afternoon on account of the rough urban surface, reducing the transmission of O_3 from the coast to the land. The expansion of lakeside cities extends the lifetime of the lake breeze from noon to afternoon. Since the lake breeze ~~can~~ accelerates the vertical mixing of O_3 in the boundary layer, the surface O_3 in lakeside cities can increase ~~by even~~as much as 30 μg m^{-3}.

(3) When the AH fluxes are taken into account, T_2, PBLH, WS_{10} and O_3 will increase by about 0.2 ℃, 75 m, 0.3 m s^{-1} and 4 μg m^{-3} in and around cities, respectively. These changes are relatively smaller compared to urban expansion, and mainly appear around ~~the~~ cities where the AH fluxes are ~~usually~~ large. In addition, unlike ~~the~~ urban expansion, AH may have a ~~quite~~ limited impact on the sea and the lake breezes. But the urban breeze circulations are found to be sensitive to AH inputs.

Studying the impacts of land use and AH forced by human activities on urban environment is fundamental in improving the urban air quality. Although this study only focuses on the YRD region, most of the results can be supported by previous studies ~~that~~ conducted in other regions around the world. As ~~more and more city~~an increasing number of city clusters composed of large and medium-sized cities are being built, ~~.~~ this~~This~~ work can provide valuable insight into the formation of O_3 pollution in ~~those~~ rapidly developing regions with unique geographical features.

Data Availability Statement.

Air quality monitoring data were acquired from a mirror of data from the official NEMC real-time publishing platform (https://quotsoft.net/air/). Meteorological data were issued by the NCDC (ftp://ftp.ncdc.noaa.gov/pub/data/noaa/isd-lite/). The FNL meteorological data were ~~acquired~~ taken from the NCEP (https://doi.org/10.5065/D6M043C6/). The MEIC data were accessible at http://meicmodel.org/. These data can be downloaded for free as long as you agree to the official instructions.

Author contributions.

CZ and MX had the original ideas, designed the research, collected the data and prepared the original draft. CZ did the numerical simulations and carried out the data analysis. MX acquired financial

support for the project leading to this publication.

Acknowledgements.

~~This work was supported by the National Key Research and Development Program of China (2018YFC0213502, 2018YFC1506404).~~ We are grateful to MEPC for the air quality monitoring data, to NCDC for the meteorological data, to NCEP for global final analysis fields and to Tsinghua University for the MEIC inventories. The numerical calculations ~~have been done~~were performed on the Blade cluster system in the High Performance Computing and Massive Data Center (HPC&MDC) of School of Atmospheric Sciences, Nanjing University. We also thank the anonymous reviewers for the constructive comments and suggestions~~ from the anonymous reviewers~~.

Financial support.

This work was supported by the Natural Science Foundation of Jiangsu Province (BK20211158) and the National Key Research and Development Program of China (2018YFC0213502, 2018YFC1506404, 2019YFA0606803).

References

Abdi-Oskouei, M., Carmichael, G., Christiansen, M., Ferrada, G., Roozitalab, B., Sobhani, N., Wade, K., Czarnetzki, A., Pierce, R. B., Wagner, T., and Stanier, C.: Sensitivity of Meteorological Skill to Selection of WRF-Chem Physical Parameterizations and Impact on Ozone Prediction During the Lake Michigan Ozone Study (LMOS), J Geophys Res-Atmos, 125, 2020.

Bergin, M. S., West, J. J., Keating, T. J., and Russell, A. G.: Regional atmospheric pollution and transboundary air quality management, Annu. Rev. Environ. Resour., 30, 1-37, 10.1146/annurev.energy.30.050504.144138, 2005.

Blaylock, B. K., Horel, J. D., and Crosman, E. T.: Impact of Lake Breezes on Summer Ozone Concentrations in the Salt Lake Valley, Journal of Applied Meteorology and Climatology, 56, 353-370, 2017.

Buchholz, S., Junk, J., Krein, A., Heinemann, G., and Hoffmann, L.: Air pollution characteristics associated with mesoscale atmospheric patterns in northwest continental Europe, Atmospheric

656 Environment, 44, 5183-5190, 10.1016/j.atmosenv.2010.08.053, 2010.
657 Chameides, W., and Walker, J. C. G.: A photochemical theory of tropospheric ozone, Journal of
658 Geophysical Research, 78, 8751-8760, 10.1029/JC078i036p08751, 1973.
659 Chen, F., and Dudhia, J.: Coupling an advanced land surface-hydrology model with the Penn State-
660 NCAR MM5 modeling system. Part II: Preliminary model validation, Monthly Weather
661 Review, 129, 587-604, 2001.
662 Chen, G., Zhao, L., and Mochida, A.: Urban Heat Island Simulations in Guangzhou, China, Using
663 the Coupled WRF/UCM Model with a Land Use Map Extracted from Remote Sensing Data,
664 Sustainability, 8, 10.3390/su8070628, 2016.
665 Chen, S. H., and Sun, W. Y.: A one-dimensional time dependent cloud model, J Meteorol Soc Jpn,
666 80, 99-118, 2002.
667 Crosman, E. T., and Horel, J. D.: Sea and Lake Breezes: A Review of Numerical Studies, Boundary-
668 Layer Meteorology, 137, 1-29, 10.1007/s10546-010-9517-9, 2010.
669 De Meij, A., and Vinuesa, J. F.: Impact of SRTM and Corine Land Cover data on meteorological
670 parameters using WRF, Atmospheric Research, 143, 351-370, 10.1016/j.atmosres.2014.03.004,
671 2014.
672 Ding, A., Wang, T., Zhao, M., Wang, T., and Li, Z.: Simulation of sea-land breezes and a discussion
673 of their implications on the transport of air pollution during a multi-day ozone episode in the
674 Pearl River Delta of China, Atmospheric Environment, 38, 6737-6750,
675 10.1016/j.atmosenv.2004.09.017, 2004.
676 Fan, H. L., and Sailor, D. J.: Modeling the impacts of anthropogenic heating on the urban climate
677 of Philadelphia: a comparison of implementations in two PBL schemes, Atmospheric
678 Environment, 39, 73-84, 2005.
679 Fast, J. D., Gustafson, W. I., Easter, R. C., Zaveri, R. A., Barnard, J. C., Chapman, E. G., Grell, G.
680 A., and Peckham, S. E.: Evolution of ozone, particulates, and aerosol direct radiative forcing
681 in the vicinity of Houston using a fully coupled meteorology-chemistry-aerosol model, J
682 Geophys Res-Atmos, 111, 2006.
683 Ferguson, G., and Woodbury, A. D.: Urban heat island in the subsurface, Geophysical Research
684 Letters, 34, 2007.
685 Flanner, M. G.: Integrating anthropogenic heat flux with global climate models, Geophysical

686 Research Letters, 36, n/a-n/a, 10.1029/2008gl036465, 2009.
687 Freitas, E. D., Rozoff, C. M., Cotton, W. R., and Dias, P. L. S.: Interactions of an urban heat island
688 and sea-breeze circulations during winter over the metropolitan area of Sao Paulo, Brazil,
689 Boundary-Layer Meteorology, 122, 43-65, 2007.
690 Friedl, M. A., Sulla-Menashe, D., Tan, B., Schneider, A., Ramankutty, N., Sibley, A., and Huang,
691 X.: MODIS Collection 5 global land cover: Algorithm refinements and characterization of new
692 datasets, Remote Sensing of Environment, 114, 168-182, 10.1016/j.rse.2009.08.016, 2010.
693 Fu, Y. and Liao, H.: Impacts of land use and land cover changes on biogenic emissions of volatile
694 organic compounds in China from the late 1980s to the mid-2000s: implications for
695 tropospheric ozone and secondary organic aerosol, Tellus B: Chemical and Physical
696 Meteorology, 66, 10.3402/tellusb.v66.24987, 2014.
697 Gao, D., Xie, M., Chen, X., Wang, T. J., Liu, J., Xu, Q., Mu, X. Y., Chen, F., Li, S., Zhuang, B. L.,
698 Li, M. M., Zhao, M., and Ren, J. Y.: Systematic classification of circulation patterns and
699 integrated analysis of their effects on different ozone pollution levels in the Yangtze River Delta
700 Region, China, Atmospheric Environment, 242, 2020.
701 Gong, P., Liu, H., Zhang, M., Li, C., Wang, J., Huang, H., Clinton, N., Ji, L., Li, W., Bai, Y., Chen,
702 B., Xu, B., Zhu, Z., Yuan, C., Ping Suen, H., Guo, J., Xu, N., Li, W., Zhao, Y., Yang, J., Yu, C.,
703 Wang, X., Fu, H., Yu, L., Dronova, I., Hui, F., Cheng, X., Shi, X., Xiao, F., Liu, Q., and Song,
704 L.: Stable classification with limited sample: transferring a 30-m resolution sample set
705 collected in 2015 to mapping 10-m resolution global land cover in 2017, Science Bulletin, 64,
706 370-373, 10.1016/j.scib.2019.03.002, 2019.
707 Grell, G. A., and Dévényi, D.: A generalized approach to parameterizing convection combining
708 ensemble and data assimilation techniques, Geophysical Research Letters, 29, 38-31-38-34,
709 10.1029/2002gl015311, 2002.
710 Grell, G. A., Peckham, S. E., Schmitz, R., McKeen, S. A., Frost, G., Skamarock, W. C., and Eder,
711 B.: Fully coupled “online” chemistry within the WRF model, Atmospheric Environment, 39,
712 6957-6975, 10.1016/j.atmosenv.2005.04.027, 2005.
713 Guenther, A., Karl, T., Harley, P., Wiedinmyer, C., Palmer, P. I., and Geron, C.: Estimates of global
714 terrestrial isoprene emissions using MEGAN (Model of Emissions of Gases and Aerosols from
715 Nature), Atmospheric Chemistry and Physics, 6, 3181-3210, 2006.

Hong, S. Y., Noh, Y., and Dudhia, J.: A new vertical diffusion package with an explicit treatment of entrainment processes, Monthly Weather Review, 134, 2318-2341, 2006.

Hu, J., Li, Y., Zhao, T., Liu, J., Hu, X.-M., Liu, D., Jiang, Y., Xu, J., and Chang, L.: An important mechanism of regional O₃ transport for summer smog over the Yangtze River Delta in eastern China, Atmospheric Chemistry and Physics, 18, 16239-16251, 10.5194/acp-18-16239-2018, 2018.

Jacob, D. J., and Winner, D. A.: Effect of climate change on air quality, Atmospheric Environment, 43, 51-63, 10.1016/j.atmosenv.2008.09.051, 2009.

Jerrett, M., Burnett, R. T., Pope, C. A., Ito, K., Thurston, G., Krewski, D., Shi, Y. L., Calle, E., and Thun, M.: Long-Term Ozone Exposure and Mortality., New Engl J Med, 360, 1085-1095, 2009.

Jiang, X., Wiedinmyer, C., Chen, F., Yang, Z.-L., and Lo, J. C.-F.: Predicted impacts of climate and land use change on surface ozone in the Houston, Texas, area, Journal of Geophysical Research, 113, 10.1029/2008jd009820, 2008.

Jimenez, P. A., and Dudhia, J.: Improving the Representation of Resolved and Unresolved Topographic Effects on Surface Wind in the WRF Model, Journal of Applied Meteorology and Climatology, 51, 300-316, 2012.

Kim, H.-J., and Wang, B.: Sensitivity of the WRF model simulation of the East Asian summer monsoon in 1993 to shortwave radiation schemes and ozone absorption, Asia-Pacific Journal of Atmospheric Sciences, 47, 167-180, 10.1007/s13143-011-0006-y, 2011.

Lennartson, G. J., and Schwartz, M. D.: The lake breeze-ground-level ozone connection in eastern Wisconsin: A climatological perspective, International Journal of Climatology, 22, 1347-1364, 2002.

Li, K., Jacob, D. J., Shen, L., Lu, X., De Smedt, I., and Liao, H.: Increases in surface ozone pollution in China from 2013 to 2019: anthropogenic and meteorological influences, Atmospheric Chemistry and Physics, 20, 11423-11433, 10.5194/acp-20-11423-2020, 2020.

Li, M., Song, Y., Huang, X., Li, J., Mao, Y., Zhu, T., Cai, X., and Liu, B.: Improving mesoscale modeling using satellite-derived land surface parameters in the Pearl River Delta region, China, Journal of Geophysical Research: Atmospheres, 119, 6325-6346, 10.1002/2014jd021871, 2014.

Li, M., Wang, T., Xie, M., Zhuang, B., Li, S., Han, Y., Song, Y., and Cheng, N.: Improved

meteorology and ozone air quality simulations using MODIS land surface parameters in the Yangtze River Delta urban cluster, China, Journal of Geophysical Research: Atmospheres, 122, 3116-3140, 10.1002/2016jd026182, 2017.

Li, Y., Zhang, J., Sailor, D. J., and Ban-Weiss, G. A.: Effects of urbanization on regional meteorology and air quality in Southern California, Atmospheric Chemistry and Physics, 19, 4439-4457, 10.5194/acp-19-4439-2019, 2019.

Liao, Z., Gao, M., Sun, J., and Fan, S.: The impact of synoptic circulation on air quality and pollution-related human health in the Yangtze River Delta region, Sci Total Environ, 607-608, 838-846, 10.1016/j.scitotenv.2017.07.031, 2017.

Lin, C. H., Lai, C. H., Wu, Y. L., Lin, P. H., and Lai, H. C.: Impact of sea breeze air masses laden with ozone on inland surface ozone concentrations: A case study of the northern coast of Taiwan, J Geophys Res-Atmos, 112, 2007.

Liu, M., and Tian, H.: China's land cover and land use change from 1700 to 2005: Estimations from high-resolution satellite data and historical archives, Global Biogeochemical Cycles, 24, n/a-n/a, 10.1029/2009gb003687, 2010.

Loveland, T. R., Reed, B. C., Brown, J. F., Ohlen, D. O., Zhu, Z., Yang, L., and Merchant, J. W.: Development of a global land cover characteristics database and IGBP DISCover from 1 km AVHRR data, International Journal of Remote Sensing, 21, 1303-1330, 10.1080/014311600210191, 2000.

Lu, X., Hong, J., Zhang, L., Cooper, O. R., Schultz, M. G., Xu, X., Wang, T., Gao, M., Zhao, Y., and Zhang, Y.: Severe Surface Ozone Pollution in China: A Global Perspective, Environmental Science & Technology Letters, 5, 487-494, 10.1021/acs.estlett.8b00366, 2018.

Mavrakou, T., Philippopoulos, K., and Deligiorgi, D.: The impact of sea breeze under different synoptic patterns on air pollution within Athens basin, Science of the Total Environment, 433, 31-43, 2012.

Menberg, K., Bayer, P., Zosseder, K., Rumohr, S., and Blum, P.: Subsurface urban heat islands in German cities, Sci Total Environ, 442, 123-133, 10.1016/j.scitotenv.2012.10.043, 2013.

Miao, Y., Hu, X.-M., Liu, S., Qian, T., Xue, M., Zheng, Y., and Wang, S.: Seasonal variation of local atmospheric circulations and boundary layer structure in the Beijing-Tianjin-Hebei region and implications for air quality, Journal of Advances in Modeling Earth Systems, 7, 1602-1626,

776 10.1002/2015ms000522, 2015.
777 Mills, G., Hayes, F., Simpson, D., Emberson, L., Norris, D., Harmens, H., and Buker, P.: Evidence
778 of widespread effects of ozone on crops and (semi-)natural vegetation in Europe (1990-2006)
779 in relation to AOT40-and flux-based risk maps, Glob. Change Biol., 17, 592-613,
780 10.1111/j.1365-2486.2010.02217.x, 2011.
781 Mlawer, E. J., Taubman, S. J., Brown, P. D., Iacono, M. J., and Clough, S. A.: Radiative transfer for
782 inhomogeneous atmospheres: RRTM, a validated correlated-k model for the longwave, Journal
783 of Geophysical Research: Atmospheres, 102, 16663-16682, 10.1029/97jd00237, 1997.
784 Oke, T. R.; Mills, G.; Christen, A.; Voogt, J. A. Urban Climates; Cambridge University Press:
785 Cambridge, 2017.
786 Park, R. J., Hong, S. K., Kwon, H. A., Kim, S., Guenther, A., Woo, J. H., and Loughner, C. P.: An
787 evaluation of ozone dry deposition simulations in East Asia, Atmospheric Chemistry and
788 Physics, 14, 7929-7940, 10.5194/acp-14-7929-2014, 2014.
789 Ryu, Y.-H., Baik, J.-J., and Lee, S.-H.: Effects of anthropogenic heat on ozone air quality in a
790 megacity, Atmospheric Environment, 80, 20-30, 10.1016/j.atmosenv.2013.07.053, 2013.
791 Sailor, D. J.: A review of methods for estimating anthropogenic heat and moisture emissions in the
792 urban environment, International Journal of Climatology, 31, 189-199, 10.1002/joc.2106, 2011.
793 Sati, A. P., and Mohan, M.: The impact of urbanization during half a century on surface meteorology
794 based on WRF model simulations over National Capital Region, India, Theoretical and Applied
795 Climatology, 134, 309-323, 2017.
796 Schell, B., Ackermann, I. J., Hass, H., Binkowski, F. S., and Ebel, A.: Modeling the formation of
797 secondary organic aerosol within a comprehensive air quality model system, J Geophys Res-
798 Atmos, 106, 28275-28293, 2001.
799 Sills, D. M. L., Brook, J. R., Levy, I., Makar, P. A., Zhang, J., and Taylor, P. A.: Lake breezes in the
800 southern Great Lakes region and their influence during BAQS-Met 2007, Atmospheric
801 Chemistry and Physics, 11, 7955-7973, 10.5194/acp-11-7955-2011, 2011.
802 Stockwell, W. R., Middleton, P., Chang, J. S., and Tang, X. Y.: The 2nd Generation Regional Acid
803 Deposition Model Chemical Mechanism for Regional Air-Quality Modeling, J Geophys Res-
804 Atmos, 95, 16343-16367, 1990.
805 Wang, H., Wu, Q., Liu, H., Wang, Y., Cheng, H., Wang, R., Wang, L., Xiao, H., and Yang, X.:

Sensitivity of biogenic volatile organic compound emissions to leaf area index and land cover in Beijing, Atmospheric Chemistry and Physics, 18, 9583-9596, 10.5194/acp-18-9583-2018, 2018.

Wang, T., Xue, L., Brimblecombe, P., Lam, Y. F., Li, L., and Zhang, L.: Ozone pollution in China: A review of concentrations, meteorological influences, chemical precursors, and effects, Sci Total Environ, 575, 1582-1596, 10.1016/j.scitotenv.2016.10.081, 2017.

Wang, X., Chen, F., Wu, Z., Zhang, M., Tewari, M., Guenther, A., and Wiedinmyer, C.: Impacts of weather conditions modified by urban expansion on surface ozone: Comparison between the Pearl River Delta and Yangtze River Delta regions, Advances in Atmospheric Sciences, 26, 962-972, 10.1007/s00376-009-8001-2, 2009.

Wang, Y., Gao, W., Wang, S., Song, T., Gong, Z., Ji, D., Wang, L., Liu, Z., Tang, G., Huo, Y., Tian, S., Li, J., Li, M., Yang, Y., Chu, B., Petäjä, T., Kerminen, V.-M., He, H., Hao, J., Kulmala, M., Wang, Y., and Zhang, Y.: Contrasting trends of $PM_{2.5}$ and surface-ozone concentrations in China from 2013 to 2017, National Science Review, 7, 1331-1339, 10.1093/nsr/nwaa032, 2020.

Wentworth, G. R., Murphy, J. G., and Sills, D. M. L.: Impact of lake breezes on ozone and nitrogen oxides in the Greater Toronto Area, Atmospheric Environment, 109, 52-60, 10.1016/j.atmosenv.2015.03.002, 2015.

~~Worden, H. M., Bowman, K. W., Worden, J. R., Eldering, A., and Beer, R.: Satellite measurements of the clear-sky greenhouse effect from tropospheric ozone, Nature Geoscience, 1, 305-308, 2008.~~

Xie, M., Liao, J., Wang, T., Zhu, K., Zhuang, B., Han, Y., Li, M., and Li, S.: Modeling of the anthropogenic heat flux and its effect on regional meteorology and air quality over the Yangtze River Delta region, China, Atmospheric Chemistry and Physics, 16, 6071-6089, 10.5194/acp-16-6071-2016, 2016a.

Xie, M., Shu, L., Wang, T.-j., Liu, Q., Gao, D., Li, S., Zhuang, B.-l., Han, Y., Li, M.-m., and Chen, P.-l.: Natural emissions under future climate condition and their effects on surface ozone in the Yangtze River Delta region, China, Atmospheric Environment, 150, 162-180, 10.1016/j.atmosenv.2016.11.053, 2017.

Xie, M., Zhu, K., Wang, T., Feng, W., Gao, D., Li, M., Li, S., Zhuang, B., Han, Y., Chen, P., and Liao, J.: Changes in regional meteorology induced by anthropogenic heat and their impacts on

air quality in South China, Atmospheric Chemistry and Physics, 16, 15011-15031, 10.5194/acp-16-15011-2016, 2016b.

Xie, M., Zhu, K., Wang, T., Yang, H., Zhuang, B., Li, S., Li, M., Zhu, X., and Ouyang, Y.: Application of photochemical indicators to evaluate ozone nonlinear chemistry and pollution control countermeasure in China, Atmospheric Environment, 99, 466-473, 10.1016/j.atmosenv.2014.10.013, 2014.

You, C., Fung, J. C. H., and Tse, W. P.: Response of the Sea Breeze to Urbanization in the Pearl River Delta Region, Journal of Applied Meteorology and Climatology, 58, 1449-1463, 2019.

Young, P. J., Archibald, A. T., Bowman, K. W., Lamarque, J. F., Naik, V., Stevenson, D. S., Tilmes, S., Voulgarakis, A., Wild, O., Bergmann, D., Cameron-Smith, P., Cionni, I., Collins, W. J., Dalsøren, S. B., Doherty, R. M., Eyring, V., Faluvegi, G., Horowitz, L. W., Josse, B., Lee, Y. H., MacKenzie, I. A., Nagashima, T., Plummer, D. A., Righi, M., Rumbold, S. T., Skeie, R. B., Shindell, D. T., Strode, S. A., Sudo, K., Szopa, S., and Zeng, G.: Pre-industrial to end 21st century projections of tropospheric ozone from the Atmospheric Chemistry and Climate Model Intercomparison Project (ACCMIP), Atmospheric Chemistry and Physics, 13, 2063-2090, 10.5194/acp-13-2063-2013, 2013.

Yu, M., Carmichael, G. R., Zhu, T., and Cheng, Y.: Sensitivity of predicted pollutant levels to urbanization in China, Atmospheric Environment, 60, 544-554, 10.1016/j.atmosenv.2012.06.075, 2012.

Zhan, C., Xie, M., Huang, C., Liu, J., Wang, T., Xu, M., Ma, C., Yu, J., Jiao, Y., Li, M., Li, S., Zhuang, B., Zhao, M., and Nie, D.: Ozone affected by a succession of four landfall typhoons in the Yangtze River Delta, China: major processes and health impacts, Atmospheric Chemistry and Physics, 20, 13781-13799, 10.5194/acp-20-13781-2020, 2020.

Zhan, C., Xie, M., Liu, J., Wang, T., Xu, M., Chen, B., Li, S., Zhuang, B., and Li, M.: Surface Ozone in the Yangtze River Delta, China: A Synthesis of Basic Features, Meteorological Driving Factors, and Health Impacts, Journal of Geophysical Research: Atmospheres, 126, 10.1029/2020jd033600, 2021.

Zhan, C.-c., Xie, M., Fang, D.-x., Wang, T.-j., Wu, Z., Lu, H., Li, M.-m., Chen, P.-l., Zhuang, B.-l., Li, S., Zhang, Z.-q., Gao, D., Ren, J.-y., and Zhao, M.: Synoptic weather patterns and their impacts on regional particle pollution in the city cluster of the Sichuan Basin, China,

Atmospheric Environment, 208, 34-47, 10.1016/j.atmosenv.2019.03.033, 2019.

Zhang, N., Zhu, L., and Zhu, Y.: Urban heat island and boundary layer structures under hot weather synoptic conditions: A case study of Suzhou City, China, Advances in Atmospheric Sciences, 28, 855-865, 10.1007/s00376-010-0040-1, 2011.

Zhang, H., Wang, Y., Hu, J., Ying, Q., and Hu, X. M.: Relationships between meteorological parameters and criteria air pollutants in three megacities in China, Environ Res, 140, 242-254, 10.1016/j.envres.2015.04.004, 2015.

Zhu, B., Kang, H., Zhu, T., Su, J., Hou, X., and Gao, J.: Impact of Shanghai urban land surface forcing on downstream city ozone chemistry, Journal of Geophysical Research: Atmospheres, 120, 4340-4351, 10.1002/2014jd022859, 2015.